American Mineralogist, Volume 86, pages 513–533, 2001

Boron metasomatism of the Alta stock contact aureole, Utah: Evidence from borates, mineral chemistry, and geochemistry

DARRELL T. WOODFORD,* VIRGINIA B. SISSON, AND WILLIAM P. LEEMAN

Department of Geology and Geophysics MS-126, Rice University, Houston, Texas 77005-1892, U.S.A.

ABSTRACT

Geochemical study of the Alta stock and adjacent contact aureole rocks provides information concerning the source, composition, and physical-chemical conditions of infiltrating fluids. Special emphasis was given to boron (B) as a tracer of fluid-rock interactions due to the occurrence of borate minerals (ludwigite, kotoite, and szaibelyite) in skarn deposits around the stock. In addition, thin section alpha-track mapping implies significant B enrichments in fluid-altered minerals within the stock, stockwork veins and related selvages, igneous sills near the stock, contact skarns, and in marbles up to 500 m from the stock. Forsterite, clinohumite, lizardite, and malachite contain between 50 and 1200 ppm B. Diopside, calcite, clintonite, phlogopite, brucite, hedenbergite, tremolite, and other minerals host B to a lesser extent. Aureole B enrichments correlate well with major and other trace-element enrichments, and support existing models of element transport in magmatic fluids with lateral down-temperature flow. Large variations in mineral B concentrations reflect changes in B concentrations of these fluids through time. Mass-balance calculations indicate that magmatic fluids emanating from the Alta pluton could supply most B in the Alta aureole. It is estimated that the emplaced magma had an initial B concentration between 7–10 ppm; indicated exhalative losses of B from the pluton are on the order of 50%. We estimate that the exsolved fluids had a time–integrated B concentration of 160 ± 40 ppm, although much higher concentrations may have attended local borate mineralization.

INTRODUCTION

Fluid infiltration is an important process during the contact metamorphism of siliceous carbonates (e.g., Moore and Kerrick 1976; Bowman and Essene 1982; Nabelek et al. 1984, 1990; Bebout and Carlson 1986; Ferry 1986, 1989, 1994; Cook and Bowman 1994; Gerdes et al. 1995; Hanson 1992, 1995a, 1995b; Cook et al. 1997; Marchildon and Dipple 1998; Dipple 1998; Ferry and Gerdes 1998; Cook and Bowman 2000). Often, the relationship between metasomatism and magmatic intrusion is controversial (Guilbert and Parks 1986; Barton et al. 1991; Skinner 1997). However, elemental and isotopic analyses of metasomatized whole-rock and mineral samples can provide important information concerning the probable source, composition, and physical-chemical condition of infiltrating fluids (Nabelek et al. 1990; Barton et al. 1991; Nabelek and Labotka 1993; Romer and Heinrich 1998).

Recent studies of the Alta stock contact aureole, Utah, have shown that fluid infiltration played an important role in heat and volatile transport during the metamorphism of siliceous carbonates (Cook 1992; Bowman et al. 1994; Ferry 1994, 1995; Cook and Bowman 1994; Hanson, 1995b; Gerdes et al. 1995; Cook et al. 1997; Marchildon and Dipple 1998; Cook and Bowman 2000). Reaction-progress calculations and finite-element modeling indicate that all metamorphic zones, including the outermost talc zone, required some fluid infiltration (Cook 1992; Ferry 1994; Cook and Bowman 2000). The Alta stock appears to be the source of infiltrating fluids based on oxygen isotopic data and field observations (Moore and Kerrick 1976; Cook 1992; Cook and Bowman 1994, 2000; Bowman et al. 1994; Cook et al. 1997), and most researchers agree that magmatic fluids infiltrated the carbonates within 200 m (periclase zone) of the stock. This study reexamines the source and nature of infiltrating fluids in terms of major- and trace-element variations in a transect across the aureole.

Boron is an especially important indicator of infiltration as borate mineralization at Alta is pervasive near the stock contact and occurs locally in metasomatic deposits. This element is highly soluble in aqueous fluids and is considered to be relatively incompatible in most rock-forming minerals (Leeman and Sisson 1996). Therefore, fluids likely control the B distribution in this system. Moreover, B contents in metasomatic minerals provide complementary information on fluid distribution patterns and the extent of fluid infiltration.

GEOLOGICAL BACKGROUND AND PREVIOUS WORK

The Alta stock is one of 11 mid-Tertiary calcalkaline intrusions in Utah's central Wasatch Mountains (John 1991; Fig. 1). The stock is a granodiorite to quartz monzodiorite body with plagioclase, perthitic K-feldspar, quartz, hornblende, and bi-

* Present address: Veritas GeoServices, 10300 Town Park, Houston, Texas 77072. E-mail: todd_woodford@veritasdgc.com

otite; accessory minerals include magnetite, titanite, apatite, zircon, and rare allanite (John 1991). The Alta stock probably is derived from a lower continental crustal source (Farmer and DePaolo 1983; Wright and Wooden 1991). The Alta stock intruded several sub-horizontal sedimentary layers ranging in age from Proterozoic to Mississippian. Basin and Range extension tilted the entire Wasatch range about 20° to the east (Grant 1966) resulting in paleodepths of the exposed stock between 6.3 km on the west to 3.7 km on the east (John 1989, 1991)

Wilson (1961), Smith (1972), Cranor (1974), Moore and Kerrick (1976), and Cook (1992) described the geology of the contact aureole. Metamorphism of siliceous dolostones from the Cambrian Maxfield, and Mississippian Deseret, Gardison, and Fitchville formations resulted in the successive appearance of talc, tremolite, forsterite, clinohumite, and periclase (Fig. 1) in massive dolostones (containing ~2.5 wt% disseminated silica). In contrast, dolostones containing chert nodules record successive growth of talc, tremolite, diopside, wollastonite, and periclase. In both lithologies, fluid X_{CO_2} increases from the talc to the forsterite zone. The absence of univariant or invariant assemblages indicates that the buffering capacity of the rocks was overwhelmed by fluid infiltration (Cook 1992). Calculated fluid X_{H_2O} increases abruptly in the periclase zone. Subsequent hydration to brucite reflects an influx of H_2O presumably from the stock. This trend also is indicated by metasomatic mineralization and replacement skarns (tactites) within the periclase zone and by stable isotope studies (Cook 1982, 1992; Kemp 1985; Bowman et al. 1994).

Inferred peak temperature conditions during intrusion and metamorphism ranged from 400 °C in the talc zone to 625 °C at the contact (Moore and Kerrick 1976; Cook 1992). Cook and Bowman (1994) calculated a stock emplacement temperature of 825 °C, which falls within the range (840–650 °C) estimated by John (1991). Metamorphic pressures (100–190 MPa), determined from metamorphic mineral assemblages and fluid inclusion data, are consistent with stratigraphically determined paleodepths (Wilson 1961; Kemp 1985; John 1991).

Because conductive heat-transfer models underestimate the spacing of reaction isograds in the southern Alta aureole, it is likely that advective heat transfer by magmatic fluid migration was important (Cook 1992). Moore and Kerrick (1976) recognized that a general increase in the OH/(F+OH) ratio of tremolite and clinohumite with increasing metamorphic grade could be attributed to mixing between the formation fluids in dolostones and infiltrating magmatic fluid. Variations in $\delta^{18}O$ values between the unmetamorphosed dolostones and various

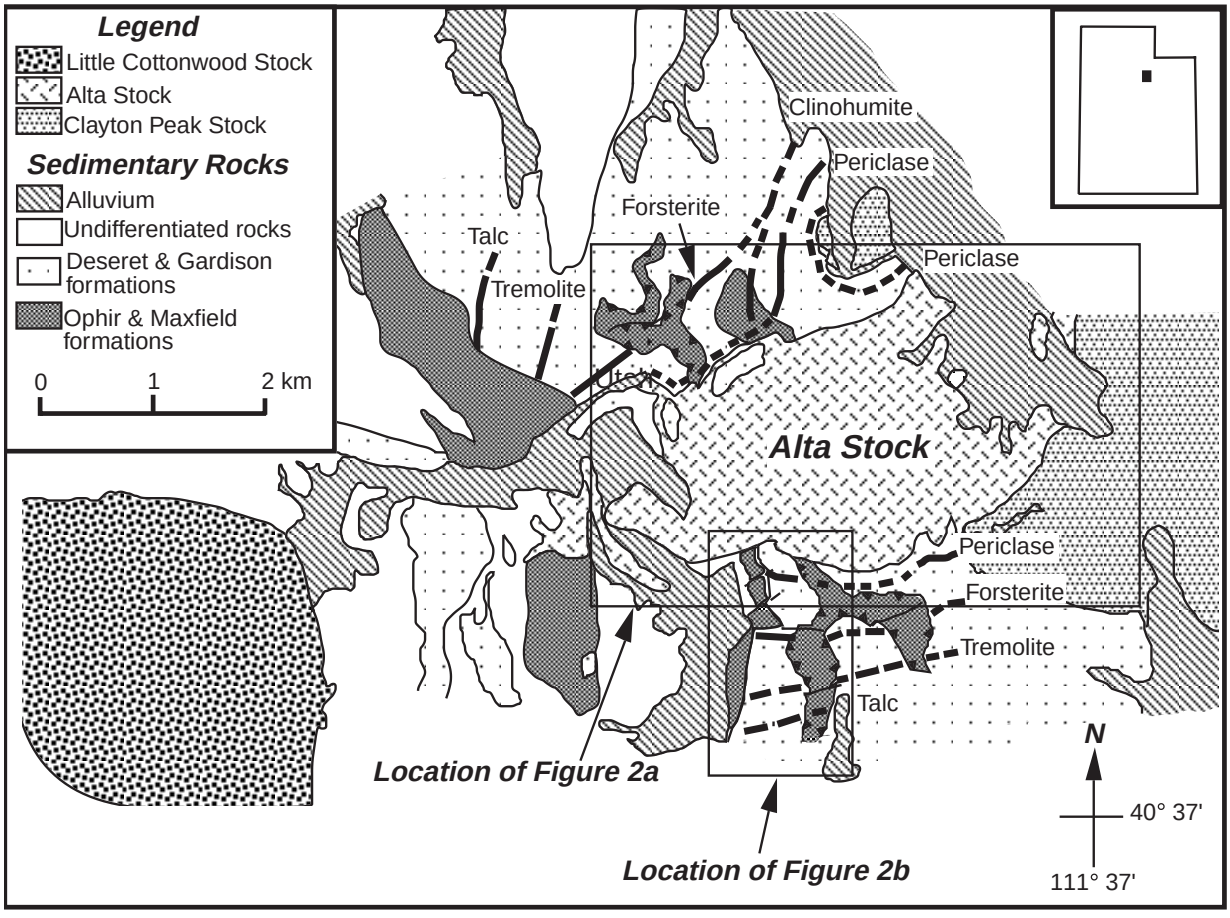

FIGURE 1. Generalized geologic map of the Alta stock and contact aureole (after Crittenden 1965; Baker et al. 1966). Mineral isograds are based on assemblages found in massive dolostone (Moore and Kerrick 1976). This study focuses on the southern contact zone shown in the boxes for Alta stock (2a) and aureole (2b).

metamorphic zones also are consistent with horizontal, down temperature magmatic fluid flow (Bowman et al. 1994; Cook et al. 1997; Cook and Bowman 2000). Bowman et al. (1994) documented that the talc, tremolite, and outermost forsterite zones lie in the rock-dominated segment of the flow path. Large ^{18}O-depletion in the periclase zone and parts of the inner forsterite zone require infiltration of ^{18}O-depleted water-rich fluids (Bowman et al. 1994; Cook et al. 1997).

Reaction-progress calculations indicate that all grades of marble were infiltrated by fluids during contact metamorphism (Cook 1992; Ferry 1994; Cook and Bowman 2000). Estimates of average time-integrated fluid flux using two-dimensional models of heat and mass transport and reaction progress indicate 4.2×10^7, 6.65×10^5, and 2.0×10^5 mol fluid/m^2 for the periclase, forsterite, and tremolite zones, respectively (Cook and Bowman 2000). The one-dimensional models of Bowman et al. (1994) and Ferry (1994) underestimate the time-integrated fluid flux for the inner aureole. Recently, Cook and Bowman (2000) documented the heterogeneous nature of fluid flow in the periclase, tremolite, and talc zones. In addition, they suggested that fluid leaked out of the flow system between the periclase and tremolite zones. In summary, these simulations of the aureole's thermal and oxygen mass-transport history match observed conditions only for subhorizontal, down-temperature fluid flow (Bowman et al. 1994; Ferry 1994; Cook et al. 1997; Cook and Bowman 2000). In addition, the Ophir shale, which stratigraphically underlies the carbonates (Fig. 2b), likely impeded vertical fluid movement.

Many small contact and fissure-type skarns are found within the marbles especially along the igneous contact. The skarns are irregularly shaped lenses, which range in thickness from 5 cm to 125 m (Cook 1982). Mineral zonation is parallel to igneous contacts and indicates outward migration of magmatic fluids, which resulted in the addition of Si, Fe, Al, and B to the wallrock. These elements were not sufficiently concentrated in the original carbonates to produce the skarns in a closed system. Cook (1982) and Kemp (1985) defined two periods of skarn formation. Stage I skarns contain prograde mineral assemblages with grandite-series garnets, clinopyroxene, and magnetite together with minor calcite and quartz. Ludwigite [$(Mg, Fe^{2+})_2Fe^{3+}BO_5$] usually forms a border zone between the skarn and dolostone (Cook 1982). Stage II skarns have retrograde mineral assemblages (epidote, actinolite, pyroxene, quartz, calcite, chlorite, scheelite, magnetite, pyrite, and ore sulfides) that either replace or crosscut Stage I assemblages. Fluid inclusion compositions and oxygen isotope data indicate that Stage I skarns are related to magmatic fluids and Stage II skarns are related to meteoric fluids (Cook 1982; Kemp 1985). A drop in hydrostatic pressure between the formation of Stage I and Stage II skarns, from near lithostatic to hydrostatic conditions, could have caused the influx of meteoric fluids (Bowman et al. 1985; Bowman 1986).

SAMPLING

Samples were collected from the Alta stock, skarns, aureole rocks, and from an equivalent unmetamorphosed lithology (Fig. 2). Igneous samples include relatively unaltered granodiorite, internal pegmatites, aplite dikes, stockwork veins, and fluid-altered granitic sills that intruded brucite marbles. Contact aureole and skarn samples were collected from the southwest side of the stock in carbonates of the Maxfield, Fitchville, and Deseret-Gardison formations. Samples of the underlying Ophir shale were collected to evaluate their possible role as source rock for fluid solutes.

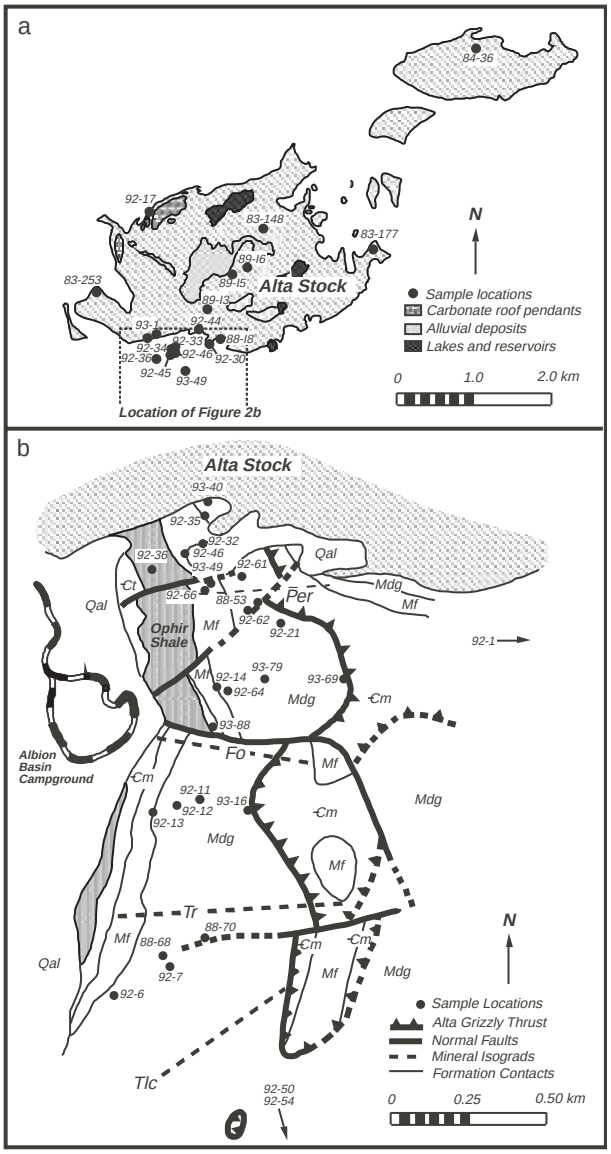

FIGURE 2. (a) Map showing locations of igneous samples from this study (Cook and Bowman unpublished data; John 1991) (geology after Baker et al. 1966). The dashed rectangular area along the southern margin corresponds to the contact aureole study area. **(b)** Map showing locations of skarn and aureole samples (geology after Baker et al. 1966; Cook 1992). Metamorphic isograds are labeled by index mineral: talc (tlc); tremolite (tr); forsterite (fo); and periclase (per). Stratigraphic units include the Cambrian Tintic (Ct), Ophir Shale, and Maxfield (Cm) formations; Mississippian Fitchville (Mf) and Deseret/Gardison (Mdg) formations and Quaternary alluvium (Qal). The Alta-Grizzly thrust (labeled with teeth) predates the Alta intrusion, and has repeated some of the stratigraphic section.

Analytical methods and results

To evaluate metasomatism at Alta and the utility of B as a tracer of fluid flow, several methods of investigation were used including inductively coupled plasma mass spectrometry (ICP-MS), X-ray fluorescence (XRF), fluid-inclusion analyses, electron-microprobe analysis, prompt gamma neutron activation analysis (PGNA), and alpha-track mapping (ATM).

Whole-rock igneous, pelitic, and carbonate samples were analyzed by XRF and ICP-MS at Washington State University GeoAnalytical Laboratory and XRAL Analytical Labs. Results are shown in Tables 1 and 2.

Fluid inclusion analyses of an igneous sill and related skarn samples were made on a FLUIDS Inc. heating-freezing stage. Analytical procedure followed that of Roedder (1984). Halite dissolution temperatures and the equations of Bowers and Helgeson (1983) and Zhang and Frantz (1987) were used to calculate wt% NaCl equivalent in primary inclusions. Fluid inclusion homogenization temperatures above 500 °C could not be measured with this apparatus.

Mineral analyses were done at Rice University using a Cameca SX-50 electron microprobe. Data reduction used PAP routines of Pouchou and Pichoir (1987). Analytical conditions include a 5 μm beam at 15 kV accelerating potential and 15 nA sample current, and counting times of 10 seconds for all elements except B and F which were counted for 30 seconds. Natural and synthetic silicate and oxide standards were used for all elements except B, for which elemental B and cubic BN were used. Recently, McGee and Anovitz (1996) have advocated the use of B standards similar to the mineral to be analyzed as well as use of lower accelerating potential (10 kV); thus, small systematic errors in microprobe B analyses could affect calculated mineral Fe^{3+}/Fe^{2+} ratios based on stoichiometry.

Alpha-track maps (ATMs) were prepared to ascertain B and Li spatial distributions in thin sections and mineral separates as described by Truscott and Shaw (1984), Truscott et al. (1986), and Shaw et al. (1988a, 1988b). Under low magnification, individual tracks are not resolved, but an aggregate track image of each mineral grain is seen. Light gray areas in Figures 6, 8–10, and 12–13 correspond to high track densities and dark gray areas to low track densities. After scanning ATMs into a digital TIFF format, Adobe Photoshop was used to enhance contrast and bring out textural features. Thus, grayscales are not directly comparable between different maps. Lithium generates tracks that are indistinguishable from those produced by B, but given terrestrial isotopic proportions, B generates 10–15 times more tracks than Li for equivalent concentrations. For these reasons, quantitative applications are problematic. A semi-quantitative technique, based on relative intensity of transmitted light through ATMs of samples and standards prior to image processing, was used to approximate the number of alpha-tracks per unit area and, thus, the maximum B content (e.g., Woodford 1995). This technique involved calibrating track-free areas as grayscale = 0 and an opaque black ink dot as grayscale = 255. The freeware computer program NIH Image was used to determine grayscale values of various track concentrations. Uncertainties include variations in densities of minerals and standards as well as statistical overlap of alpha-tracks. This technique does not work well for high B samples as the algorithms used are not sensitive for grayscale values above 200. The greatest source of uncertainty is the presence of unknown amounts of Li. In general, the estimated error is approximately ±20% for most minerals, but may be greater in diopside and micas, which tend to have higher Li contents.

Quantitative analysis of B in whole-rock powders and mineral separates was done using prompt gamma neutron activation analysis (PGNA). This technique was described by Truscott et al. (1986) and Shaw et al. (1988b). Mineral separates were prepared using standard heavy liquid techniques with Na-polytungstate solutions followed by hand separation. Shaw et al. (1988a) used Na-polytungstate for mineral separations and report no detectable B contamination from its use. The detection limit varies with the nature and size of a sample, but is on the order of 0.3 ppm for a 2 g sample. Precision varies between ±10% for low B content (<10 ppm) to ±5% for higher B contents (Truscott and Shaw 1984; Shaw et al. 1988a, 1988b). Sample sizes of up to 0.25 g were used for B analysis of mineral separates (Table 3).

Fluid Inclusion data

Several generations of fluid inclusions have been documented within the Alta stock and associated skarns (John 1991; Kemp 1985). In order to verify that similar fluids were present within our samples, we analyzed fluid inclusions in a granitic sill (92A-33H) and associated skarn (92A-33G). In both the sill and skarn, the primary inclusions contained salt daughter crystals; moreover, there were opaque (magnetite?) daughter crystals in the skarn fluid inclusions. Homogenization temperatures range widely from 130 to >500 °C (Fig. 3). Salinities determined from halite dissolution temperatures range from 30 to 70 wt% NaCl equivalent and average 35 wt% NaCl equivalent.

Major and trace element geochemistry

Variation in protolith geochemistry of the dolostones must be assessed before quantifying any metasomatic chemical changes (e.g., Nabelek and Labotka 1993). Principle component analysis of the unmetamorphosed and talc zone samples was used to evaluate causes of chemical variation; all analyses were first recalculated to 100% totals on a volatile-free basis. Because 99% of the chemical variation can be attributed to CaO and MgO, we conclude that heterogeneities in the protolith are due largely to differences in modal proportions of dolomite and calcite. A minute fraction of the variance in the second principle component is due to SiO_2 and Al_2O_3, which can be attributed to small variations in quartz, mica, feldspar, or other aluminosilicate mineral components.

First-order compositional variations in the aureole carbonates include small enrichments of Si, Al, Fe, and Ca, and a depletion of Mg approaching the contact (Fig. 4a). Although element mobility commonly is evaluated with respect to an immobile element (e.g., Al or Ti), the TiO_2 content in most Alta marbles is negligible; thus, we only consider normalization to Al_2O_3. Moreover, to minimize influence of protolith variation, we used averaged analyses of each mineral zone (Table 2). Relative to Al_2O_3, the other major elements (Ca, Mg, Fe, Si, and K) tend to decrease toward the contact (Fig. 4b). This behavior belies the common assumption that Al is rela-

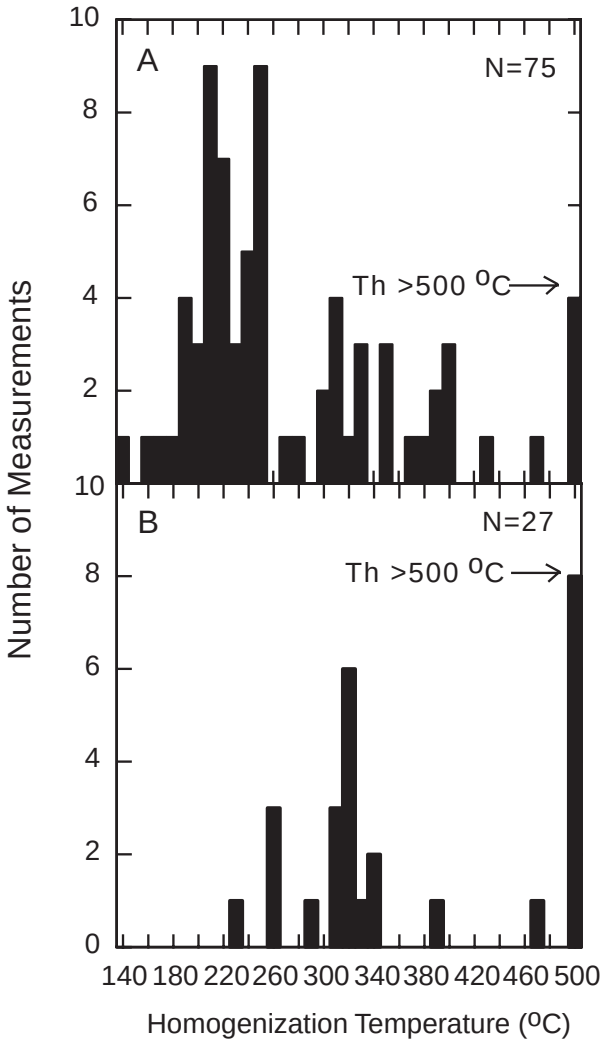

FIGURE 3. Histogram of fluid inclusion homogenization temperatures in **(a)** granitic sill 92A-33H, and **(b)** the adjacent garnet diopside skarn zone located 8 cm away. Inclusions plotted at 500 °C actually have higher homogenization temperatures, which could not be measured with our apparatus. The wide scatter in both plots indicates that several generations of fluid infiltrated the rock. The highest temperature inclusions are primary and have very high salinities (30–70 wt% NaCl equivalent) and are interpreted to be exsolved magmatic fluids. Lower temperature inclusions are secondary.

tively immobile under metamorphic conditions. Selected trace elements also exhibit systematic gradients with B, Ni, V, Zr, Sr, Sc, La, and Y (REE) generally increasing toward the contact (Fig. 4c–4f), whereas the REE contents (also Si, Al, Fe) seem to decrease sharply in periclase zone rocks. This small irregularity may be an artifact of including in the forsterite zone average several samples with anomalous enrichments in K, Al, Ti, Fe, and F. These latter samples contain phlogopite and chondrodite as well as accessory spinel, titanite, and pyrite, and presumably reflect local metasomatism or anomalous protolith compositions. Multi-element diagrams showing compositions normalized to either unmetamorphosed dolostone or talc-zone samples exhibit similar patterns in which the fluid mobile elements B and Sr are enriched in the periclase and forsterite zones (Fig. 5). In addition, Zr, Nb, and Ce may be enriched in the inner aureole. Other analyzed elements do not vary systematically throughout the Alta aureole.

Rocks from the Alta pluton exhibit typical igneous fractionation trends, with the exception of highly differentiated sills injected between carbonate layers (Table 1). The variable compositions of these sills indicate alteration either by loss of a volatile component into the carbonate host rocks or alteration by magmatic fluids. Significant B enrichments are observed in sills associated with ludwigite-bearing skarns.

BORON DISTRIBUTION IN ROCKS AND MINERALS FROM ALPHA-TRACK MAPPING

Alpha-track maps were studied in conjunction with corresponding thin sections to determine host minerals for and the textural distribution of B (+ Li). Minerals in Alta igneous rocks show decreasing track densities in the order: sericite > plagioclase in sills > biotite > amphibole > plagioclase in the stock = quartz. In the skarns, boron concentrations are sufficiently high in some minerals (e.g., borates) to saturate the ATMs; thus, corresponding track densities may appear less intense (darker) than silicate minerals containing less boron. The relative track densities for skarn minerals decrease in the order: forsterite = serpentine > diopside > clintonite > wollastonite = plagioclase > phlogopite > garnet = magnetite = spinel. In the metamorphic aureole, track intensity decreases in the order: forsterite = serpentine = clinohumite = chondrodite > calcite in inner aureole > brucite = tremolite > talc > calcite in outer aureole.

Igneous rocks and minerals

Figure 6a shows a representative stock sample (89-I5). Plagioclase, quartz, titanite, and magnetite host negligible B. Note that variable track density in plagioclase grains reflects varying degrees of sericite alteration. Biotite and sericite (altered feldspar) both have high track densities and host B; because analyses of biotite separates from the stock reveal low B contents (0.5 to 4.5 ppm), some of the alpha-tracks may be produced by Li. The whole-rock sample contains 4.4 ± 0.4 ppm B. As the biotite modal abundance is 5–10%, biotite contains no more than 10% of the total B. Therefore, we infer that most of the B is contained in sericitic alteration products. Although sericite could not be analyzed directly due to its very fine grain size, its B content is high (>100 ppm) as estimated from sericite modal abundance and whole-rock B concentrations. Less common hornblende has a moderate track density corresponding to a B concentration of <6 ppm.

Small (<15 cm thick), essentially fresh pegmatite and aplite dikes are common within the Alta Stock (John 1991). Biotite separates for these rocks contain little B (less than the 0.5 ppm detection limit). The B content in feldspar (~3 ppm) is consistent with data from other locations (e.g., Leeman and Sisson 1996). Low whole-rock B concentration in aplite (2.9 ppm vs. the average stock value of 4.4 ppm) may be consistent with exhalative loss of B from these melts (Fig. 7).

John (1991) described seven distinct stages of stockwork vein generation at Alta and deduced their relative sequence of

TABLE 1. Major and trace element composition of Alta rocks*

Sample	88-I8 stock†	88-I10 stock†	89-I3 stock†	89-I5 stock†	89-I6 stock†	89-I10 stock†	92A-44D stock	92A46 granophyre
distance (km)								0.10
SiO_2 (%)	57.70	65.50	61.50	64.20	64.60	64.40	63.80	77.23
Al_2O_3	17.80	15.80	16.50	16.10	16.10	16.30	16.54	12.32
TiO_2	0.78	0.51	0.62	0.57	0.52	0.57	0.60	0.033
FeO	6.53	4.06	4.96	4.51	4.20	4.32	4.45	0.33
MnO	0.12	0.09	0.10	0.09	0.09	0.09	0.09	0.005
CaO	6.20	3.91	4.64	4.09	3.78	4.03	4.29	0.79
MgO	2.91	1.93	2.09	1.99	1.80	1.89	1.87	0.04
K_2O	2.54	3.57	3.05	3.37	3.49	3.34	3.57	7.56
Na_2O	4.02	3.74	4.14	3.95	3.95	4.07	3.94	2.31
P_2O_5	0.43	0.22	0.30	0.25	0.23	0.25	0.32	0.004
LOI								
Total	99.03	99.33	97.90	99.12	98.76	99.26	99.47	100.62
Ni	10	11	13	9	12	10	12	12
Cr	8	37	34	9	37	13	14	10
Sc		8.0	8.0		7.0		8.0	5.0
V		61	77		66		84	
Ba	1500	1300	1400	1400	1400	1600	1618	304
Rb	70	100	110	120	120	110	113	339
Sr	1200	770	970	810	820	860	740	159
Zr	220	180	200	170	170	180	203	56
Y	10	10	20	10	10	10	17	1.7
Nb	30	10	20	20	10	10	14	3.4
Cu	15	6	25	10	9	9	250	25
Zn	40	46	100	38	48	35	53	7
Pb		12	14		10		18	6.9
La		62	55		48		66	10.4
Ce		100	96		81		108	14.4
Th	10	18	11	13	10	14	12	14.9
B							4.4	50

TABLE 1. *—Continued*

	88-A7 forsterite†	88-12 forsterite†	88-53 forsterite†	88-60 forsterite†	88-16A forsterite†	88-55 forsterite†	92A-64 forsterite	88-22 forsterite†	88-59 clinohumite†
distance (km)	0.11	0.12	0.38	0.40	0.40	0.49	0.51	0.54	0.55
SiO_2 (%)	3.84	1.10	0.44	1.82	8.06	6.63	7.52	0.19	1.17
Al_2O_3	1.01	0.41	0.04	0.37	0.08	2.10	1.69	0.01	0.06
TiO_2	0.05	0.03	0.00	0.01	0.01	0.09	0.09	0.00	0.00
FeO	0.28	0.20	0.06	0.26	0.14	0.77	0.51	0.01	0.01
MnO	0.01	0.04	0.01	0.01	0.01	0.01	0.01	0.02	0.01
CaO	45.20	31.80	50.50	46.70	35.50	31.80	32.90	31.50	49.80
MgO	10.40	22.20	6.16	8.52	16.60	18.50	18.27	22.20	6.31
K_2O	0.01	0.01	0.01	0.05	0.02	0.46	0.25	0.01	0.03
Na_2O	0.03	0.03	0.03	0.02	0.03	0.07	0.00	0.03	0.04
P_2O_5	0.02	0.01	0.05	0.01	0.01	0.02	0.01	0.01	0.01
LOI	39.30	44.10	41.70	41.30	39.10	38.20	38.74	46.40	43.00
Total	100.15	99.93	99.00	99.07	99.56	98.65	99.99	100.38	100.44
Ni	5	3	8	3	2	8		1	1
Cr	2			7		7	15		6
Sc		0.4	0.1						
V		8	28				21		
Ba						20	19		
Rb		10	10	20	10	30	8		
Sr	330	60	370	380	70	150	186	50	330
Zr	20						36		
Y							4		
Nb							2		
Cu	14	97		1.3					
Zn		52	14			10	36		3.7
Pb		48	10	2			11	6	
La		1.4	6.7				3		
Ce		2	3				5		
Th	0.6	0.5		0.7		1.5	1		
B	41		0.5		28	38	15.9		10.0

* Oxides in wt%, trace elements in ppm.
† Data from Cook (1992) and Cook and Bowman (2000, unpublished data).

TABLE 1. —*Extended*

92A-34 sill	92A-45C sill	92A-45D sill	92A-33H sill	92A-33A skarn	92A-33B skarn	92A-33D skarn	92A-33E skarn	88-40 periclase†	92A-61 periclase	88-51 periclase†	88-B6 periclase†	88-14 periclase†
0.10	0.10	0.10	0.08	0.08	0.08	0.08	0.08	0.01	0.15	0.18	0.20	0.24
63.67	73.48	61.19	56.11	1.24	2.34	47.33	16.36	1.79	1.59	1.17	5.40	1.27
15.20	13.27	12.45	16.02	0.09	0.83	7.32	3.53	0.13	0.15	0.31	0.41	0.13
0.59	0.19	0.57	1.08	0.00	0.017	0.120	0.080	0.00	0.00	0.01	0.03	0.00
4.12	0.67	3.32	9.67	0.44	14.58	3.26	49.87	0.05	0.00	0.46	0.25	0.24
0.06	0.02	0.10	0.08	0.06	0.097	0.106	0.596	0.01	0.01	0.01	0.02	0.03
4.92	2.52	7.45	4.97	36.14	47.04	23.28	1.41	40.10	50.96	36.20	40.90	35.70
1.87	0.43	2.67	3.37	22.99	15.88	18.46	17.61	17.00	4.31	22.10	14.90	23.30
3.83	4.65	5.94	3.80	0.00	0.01	0.20	0.01	0.02	0.02	0.01	0.01	0.00
3.51	3.65	2.82	3.27	0.00	0.00	0.00	0.00	0.02	0.00	0.02	0.05	0.02
0.30	0.08	0.31	0.69	0.00	0.004	0.079	0.047	0.01	0.01	0.01	0.02	0.08
				39.03	19.00		10.00	40.70	42.96	39.40	38.70	39.20
98.07	98.96	96.82	99.06	99.99	99.80	100.16	99.51	99.83	100.01	99.70	100.69	99.97
13	8	20	18					7		1	7	23
16		23	48		8		11	10		3	10	2
9.0	2.0	10.0	13.0		13.0	18.0	9.0	0.2			0.5	
70	6	79	221	8	30	19	125	13	23			
2088	970	1673	1095	2		19	9	10	5			
109	107	144	155			18		10				
799	429	507	548	114	154	27	13	190	420	270	180	150
209	53	139	341	15	31	73	30		28			
20	10	34	21	1	4	5	3		1			
14	12	27	14	1	22.9	6.3	5.7	10			10	
18	27	2	169	6	321	442	25139				3.2	
24	9	32	46	198	213	105	1539	15		30	47	130
15	10	11	12		5	4	5	2	1			
66	21	54	36	2	23	14	12	1.7	1		2.3	
117	43	118	64	2	12	50		2			3	
11	18	8	10			6	1	0.11		0.4		0.2
10.1	23.3	19.0	10.3	24		77	215	22	6.0	29	36	20

TABLE 1. —*Extended*

92A-14 forsterite	92A-14N forsterite	88-C5 forsterite†	88-25B forsterite†	88-77 tremolite†	92A-12 tremolite	92A-13 tremolite	89-39B talc†	88-70 talc†	88-68 talc†	92A-54 carbonate	92A-50 shale
0.58	0.58	0.59	0.69	0.90	0.96	0.97	1.33	1.33	1.56	2.62	3.00
4.97	1.83	6.41	5.59	1.57	1.65	1.97	1.48	1.03	0.78	2.03	64.23
1.02	0.27	1.82	1.74	0.05	0.14	0.20	0.21	0.01	0.08	0.36	13.60
0.05	0.00	0.09	0.09	0.00	0.00	0.00	0.02	0.00	0.01	0.00	0.52
0.65	0.17	0.41	0.26	0.06	0.00	0.02	0.08	0.05	0.07	0.32	7.03
0.02	0.02	0.02	0.01	0.02	0.02	0.03	0.02	0.02	0.03	0.04	0.59
33.81	44.69	31.60	32.20	32.00	32.13	32.59	31.30	31.40	31.70	31.66	2.76
17.72	9.37	21.00	18.10	20.70	19.63	19.58	21.40	21.70	21.90	19.42	1.28
0.34	0.09	0.27	0.30	0.02	0.02	0.02	0.02	0.01	0.02	0.08	5.27
0.00	0.00	0.05	0.06	0.02	0.00	0.00	0.02	0.02	0.02	0.00	0.05
0.01	0.01	0.02	0.02	0.04	0.01	0.01	0.02	0.02	0.02	0.01	1.90
41.42	43.54	37.50	41.40	45.70	46.40	45.58	45.00	45.00	44.90	46.07	3.00
100.01	99.99	99.19	99.77	100.18	100.00	100.00	99.57	99.26	99.53	99.99	100.23
		4	3	4				1	4		
9	2	2	6		2	2	5	5		1	53
				0.2					0.2		
19	9			28	17	14			13		38
18	7				11	12				5	693
9	3	10	10			1	10	10	20	2	160
133	215	80	80	60	50	59	30	30	80	64	297
26	23	20	20		14	15				17	342
4	3				4	3				1	121
1	1	10			1	1				1	18
23		1.8		2.9	2	1		7.9			47
1	1		6			4			6	4	15
3	4			2.1	1	2			1.9	1	
5	6			1		1			1	1	
1		1.8	1.4				0.2				20
11.7	3.7	14.0	0.5	0.5	1.6	0.5	0.5	0.5	0.5	1.7	93

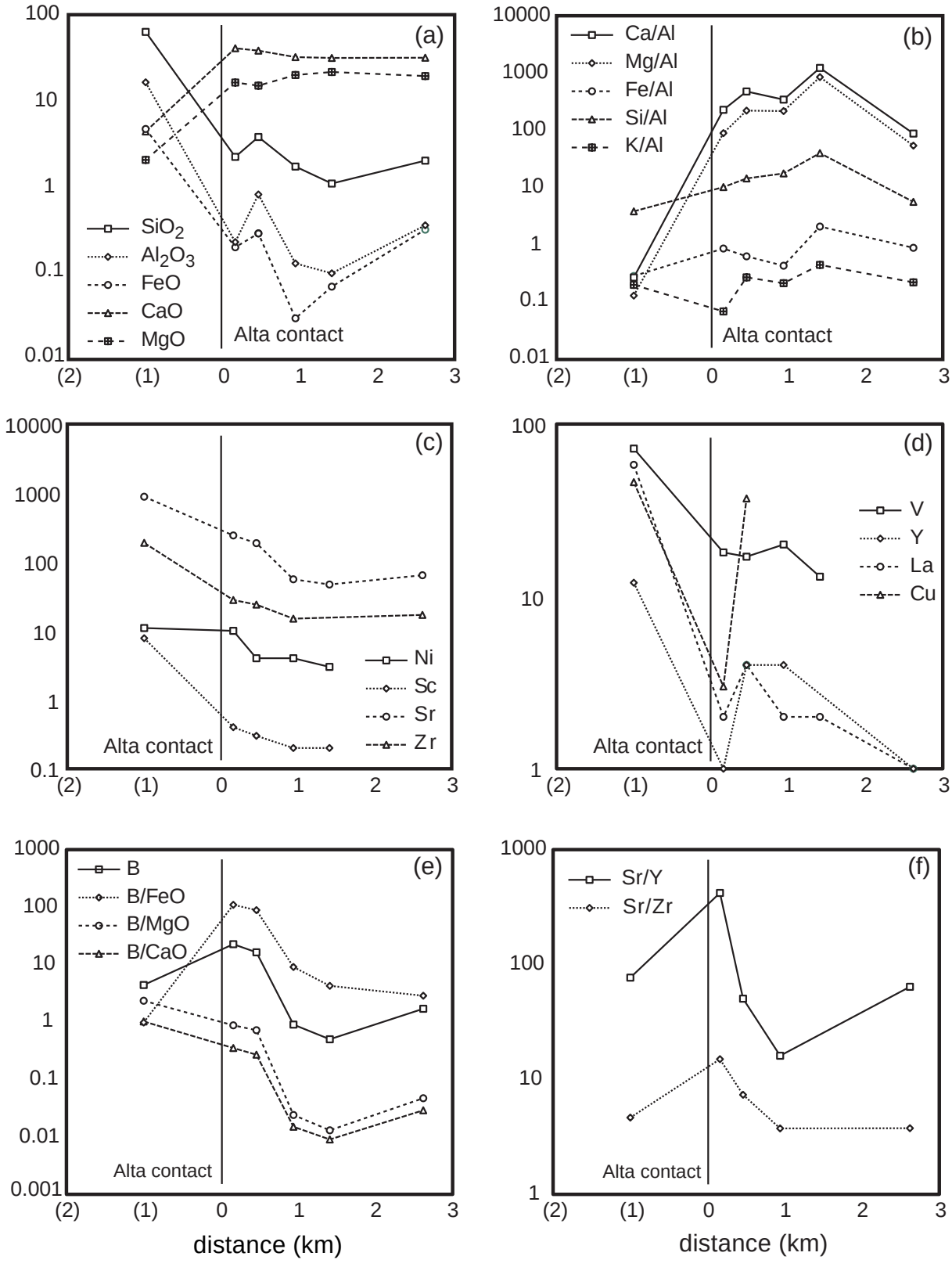

FIGURE 4. Major and trace element variations in igneous and dolostone samples across the Alta contact aureole. Plotted points represent average compositions of samples from the Alta pluton (negative distance) and metamorphic zones (positive distances), respectively, as a function of average distance from the igneous contact. Plotted major oxide data are recalculated to total 100% on a volatile-free basis.

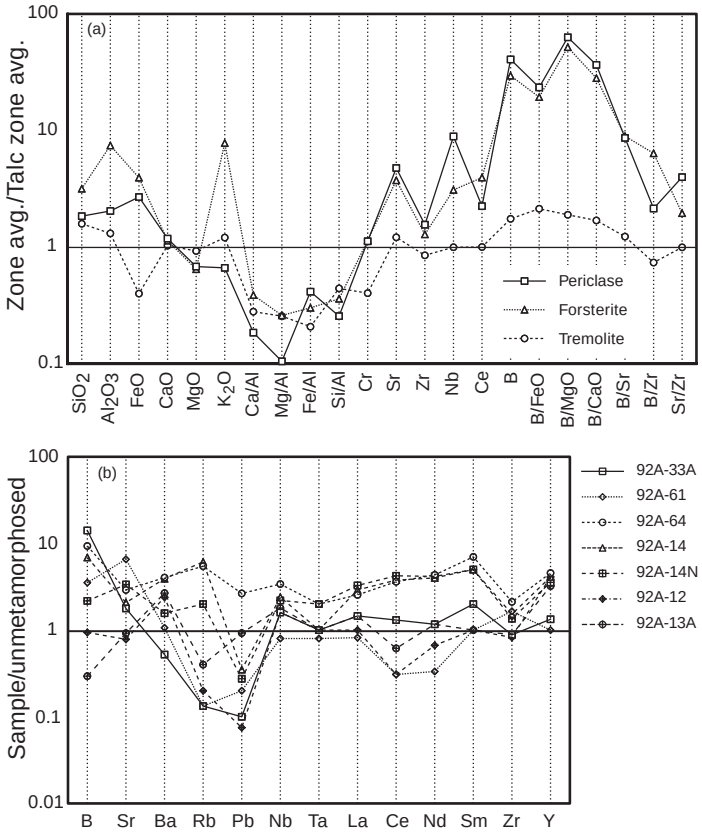

FIGURE 5. Multielement diagrams for the Alta contact aureole. **(a)** Relative abundance and element ratios for average periclase-, forsterite-, and tremolite-zone dolostones as normalized to average talc-zone composition (cf., Table 2). Where talc-zone data are lacking, composition of unmetamorphosed carbonate (92A-54) was used for normalization. **(b)** Relative abundance of selected elements for individual samples done by ICP-MS as normalized to unmetamorphosed carbonate. The samples are listed in increasing distance from the contact with the Alta stock.

TABLE 2. Average compositions* of Alta rock groups

	Alta stock		Periclase zone		Forsterite zone		Tremolite zone		Talc zone		Unmetamorphosed
	avg	±sd	avg	±sd	avg	±sd	avg	±sd	avg	±sd	
SiO_2 (%)	63.10	2.68	2.24	1.78	3.81	2.85	1.73	0.21	1.10	0.35	2.03
Al_2O_3	16.45	0.65	0.23	0.13	0.82	0.78	0.13	0.08	0.10	0.10	0.36
TiO_2	0.60	0.09	0.01	0.01	0.04	0.04	0.00	0.00	0.01	0.01	0.00
FeO	4.72	0.85	0.20	0.18	0.29	0.24	0.03	0.03	0.07	0.02	0.32
MnO	0.10	0.01	0.02	0.01	0.02	0.01	0.02	0.01	0.02	0.01	0.04
CaO	4.42	0.83	40.77	6.14	38.31	7.69	32.24	0.31	31.47	0.21	31.66
MgO	2.07	0.38	16.32	7.56	15.03	5.99	19.97	0.63	21.67	0.25	19.42
K_2O	3.28	0.37	0.01	0.01	0.14	0.16	0.02	0.00	0.02	0.01	0.08
Na_2O	3.97	0.13	0.02	0.02	0.03	0.02	0.01	0.01	0.02	0.00	0.00
P_2O_5	0.29	0.07	0.03	0.03	0.02	0.01	0.02	0.02	0.02	0.00	0.01
LOI			40.19	1.71	41.21	2.60	45.89	0.44	44.97	0.06	46.07
Total	98.98	0.53	100.04	0.38	99.70	0.56	100.06	0.10	99.45	0.17	99.99
Ni	11	1	10	9.4	3.8	2.6	4.0	–	2.5	2.1	–
Cr	22	14	6	4.3	6.2	4.2	2.0	–	5.0	–	1
Sc	7.8	0.5	0.37	0.22	0.3	0.2	0.2	–	0.2	–	–
V	72	10	18	7.1	17	8	20	7	13	–	–
Ba	1460	117	8	3.5	16	6	12	1	–	–	5
Rb	106	17	10	–	12	8	1	–	13	6	2
Sr	881	159	242	109	187	125	56	6	47	29	64
Zr	189	19	28	–	24	6	15	1	–	–	17
Y	12	4	1.0	–	3.7	0.6	3.5	0.7	–	–	1
Nb	16	8	10	–	3.5	4.4	1.0	–	–	–	1
Cu	46	90	3	–	37	52	–	–	–	–	–
Zn	51	22	56	51.4	20	18	2.0	1.0	8	–	–
Pb	14	3	1.5	0.7	11	16	4	–	6	–	4
La	58	8	1.7	0.7	3.6	2.0	1.7	0.6	2	–	1
Ce	96	11	2.5	0.7	4.2	1.6	1.0	–	1	–	1
Th	13	3	0.24	0.15	1.06	0.47	–	–	–	–	–
B	4.4	0.4	22.6	11.2	16.3	14.7	0.9	0.6	0.5	–	1.7

* Oxides in wt%, trace elements in ppm.

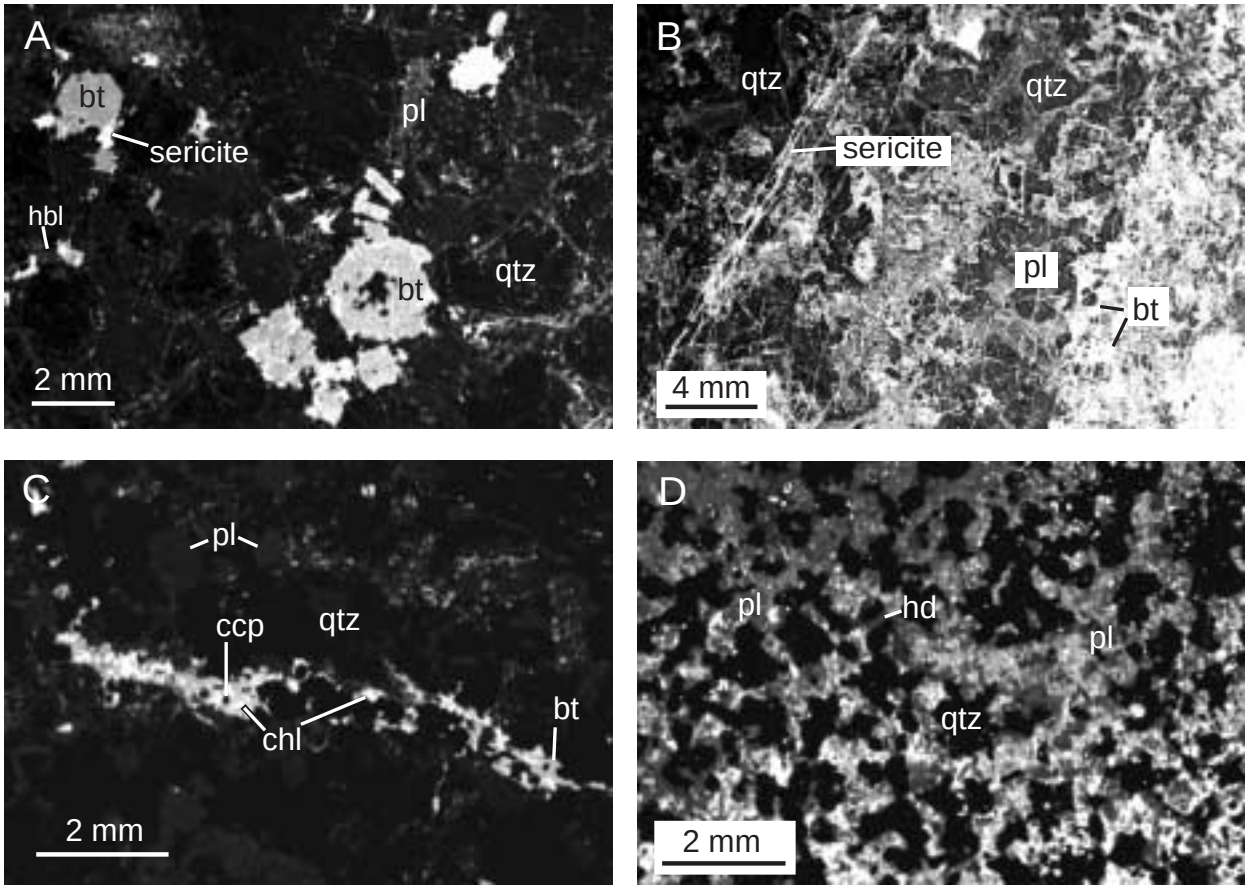

FIGURE 6. Alpha-track maps (ATMs) of Alta igneous rocks. **(a)** Alta stock (89-I5). High track densities are associated with minor sericitic feldspar alteration and biotite chloritization. Biotite has a relatively high track density (most likely due to the presence of Li), but contains less than 5 ppm B. Hornblende is associated with alpha-tracks and also contains 5 ppm B. Feldspar and quartz host little or no B. **(b)** Sill (92A-33H). The whole-rock B concentration is 10 ppm. High track concentrations are seen in biotite along the right side of the image, but again biotite separates contain only 2 ppm B indicating track contributions from Li. High track concentrations also are associated with sericitic feldspar alteration and chloritic hornblende alteration (not shown on figure). Low track concentrations are seen in feldspar and quartz. **(c)** Stockwork (83-148; cf., John 1991). High track concentrations within the vein are associated with alteration of a Cu sulfide phase. Boron content of the vein is about 100 ppm. Biotite also occurs in the vein and produces some tracks. High track concentrations in the matrix are due mainly to sericitic alteration of feldspar. **(d)** Hedenbergite sill (92A-45B). Hedenbergite contains 16 ppm B. The whole-rock B concentration is about 20 ppm. Altered plagioclase hosts most of the B present in the sample; quartz hosts none. An adjacent layer of ludwigite skarn indicates that B-rich fluids were channeled along the sill. (bt = biotite; pl = plagioclase; qtz = quartz; chl = chlorite; ccp = chalcopyrite; hd = hedenbergite; hbl = hornblende).

formation based on crosscutting relationships. Fluid inclusion and oxygen isotope data suggest that vein types 1 through 6 were derived from fluids exsolved from the stock whereas type 7 veins formed during an incursion of meteoric water. PGNA and/or ATM analysis shows that, except for type 2 veins (not analyzed), magmatically derived vein types generally have relatively high B. The selvage zones adjacent to these veins commonly have high alpha-track densities signifying exhalation of B from the veins; an exception is type 3 veins in which tracks are concentrated in vein minerals. For example, in a 2 mm thick type 1 vein (sample 92A-44C), which consists predominantly of chlorite with a pronounced ~10 mm selvage of altered feldspar, chlorite contains 6 ppm B whereas the vein + selvage combination contains 19 ppm B. In contrast, unaltered granodiorite (sample 92A-44D) collected a few centimeters away contains only 4.4 ppm B. Another example is a type 6 vein (sample 84-PC-36) with an altered feldspar selvage; the B concentration of the vein + selvage (11 ppm) is higher than the unaltered host rock (4.9 ppm). The highest B concentrations are noted in type 3 vein alteration minerals (Fig. 6c), which contain about 100 ppm B.

In the southern part of the Alta aureole, several granitic to granophyric sills intruded the country rocks at distances up to 150 m from the contact. The sills are usually less than 2 m thick, but may be as thin as a few centimeters and are typically surrounded by zoned replacement skarns (cf., Cook 1982; Kemp 1985). Figure 6b shows a small granitic sill (sample 92A-33H) that is mineralogically and texturally heterogeneous. The border zone consists of mafic minerals (chiefly biotite + hornblende) whereas the interior contains pegmatitic quartz and

feldspar, hornblende, and titanite. The whole-rock B content (10 ppm) is greater than the average stock value (Fig. 7). The sill is crosscut by B-rich micro-veins. Extensive alteration of the feldspar and mafic phases indicates fluid infiltration. High alpha-track concentrations are seen in border-zone biotite, although biotite separates contain only 2.2 ppm B. Feldspar and hornblende also are associated with alpha-tracks, especially where they have been altered to sericite or chlorite. Thus, B in the sills is mainly contained in alteration products, as it is in the stock.

More evolved sills have even higher B contents (up to 50 ppm)—again, hosted by alteration minerals. A hedenbergite-rich sill (92A-45) contains about 20 ppm B, predominantly in altered feldspar and to a lesser extent in pyroxene (Fig. 6d).

The largest of these sills is located in the Ophir formation. Tonalite sills within this formation have a pegmatitic texture and are not associated with skarn mineralization. Quartz from these sills contains 2 ppm B, which likely is hosted in fluid inclusions.

Contact metamorphic rocks and minerals

Unmetamorphosed dolostone (sample 92A-54) at 2500 m from the Alta stock contains 1.7 ppm B; it can reasonably be assumed that marbles throughout the aureole had similarly low pre-metamorphic concentrations. Progressive metamorphism of nodular siliceous dolostone of the Fitchville and Deseret-Gardison formations produced talc rims on chert nodules. The extent of the dolomite + chert reaction varies. In some stratigraphic layers there is complete reaction to talc + calcite whereas adjacent layers may contain little or no talc. Talc-zone rocks have B contents similar to the unmetamorphosed dolostone. Figure 8a shows that the B is associated with talc. Talc separated from nodular dolostone contains about 3 ppm B.

The tremolite zone has either a dolomite + tremolite assemblage in nodular dolostones, or a calcite + tremolite assemblage in massive dolostones. Tremolite also occurs in fibrous masses up to 5 cm thick and 15 to 50 cm long parallel to bedding, suggesting a derivation from pre-metamorphic chert layers. In nodular dolostone, tremolite contains essentially all the B (Fig. 8b). Massive tremolite-zone samples contain up to 2 ppm B, whereas tremolite itself contains 6–14 ppm. Higher B concentrations occur in tremolite collected near the Alta Grizzly Thrust.

Two distinct modes of forsterite occur in the Alta aureole: metamorphic and metasomatic. Metamorphic forsterite occurs as elongate pseudomorphs after tremolite (Moore and Kerrick 1976). Metasomatic forsterite is formed from Mg- and Si-rich fluids in skarns and carbonate beds near igneous contacts. Texturally, metasomatic forsterite has a short prismatic habit, high modal abundance, and is associated with other metasomatic minerals (e.g., ludwigite and spinel). Sample 92A-32 contains metamorphic and metasomatic forsterite, both of which con-

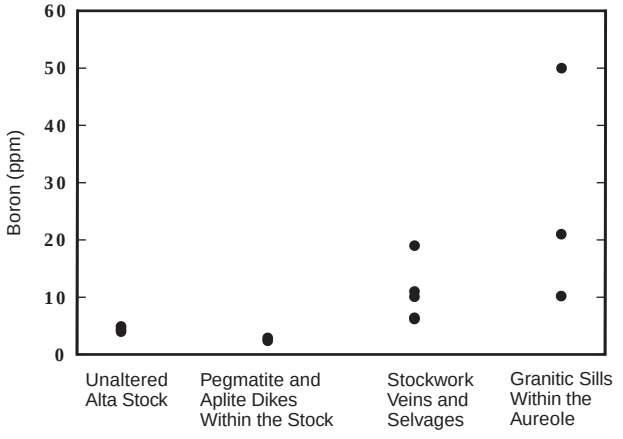

FIGURE 7. Variation in whole-rock B contents of Alta igneous rocks. The main body of the stock averages 4.4 ppm B. Pegmatites and aplites within the stock have even lower B contents. Stockwork veins and aureole sills are fluid altered and enriched in B relative to the main body of the stock. Data are from Table 1 and Woodford (1995).

TABLE 3. Boron contents in Alta bulk rocks and mineral separates

Material	Sample	ppm B
biotite-stock	92A-17	4.5
biotite-stock	92A-44D	0.5
biotite-pegmatite	92A-30	0.5
biotite-sill	92A-33H	2.2
biotite-sill	92A-34	4.0
brucite	93A-40	7.0
calcite	88-A7	1*
calcite	92A-32	11.8
calcite-skarn	92A-33F	39
chlorite-type 1 vein	92A-44C	6.0
clinohumite	88-14	400*
clinohumite	92A-62	180*
clinohumite	92A-66	25
clinohumite	93A-35F	1152
clinozoisite-endoskarn	93A-1	5.0
clintonite	92A-33D	43
diopside-skarn	92A-1A	43
diopside-skarn	92A-33D	51
diopside-skarn	92A-46	67
diopside-skarn	93A-49F	31
dolomite	92A-62	2.0
forsterite	88-A7	450*
forsterite	92A-14	102
forsterite	92A-21	95*
forsterite	92A-32	1374
forsterite	92A-62	45*
forsterite	92A-64	102
forsterite	93A-35F	1270
forsterite-skarn	92A-33E	631
hedenbergite-sill	92A-45B	16.3
hornblende-stock	92A-44D	3*
hornblende-sill	92A-33H	6*
hornblende-sill	92A-34	8*
K-spar-pegmatite	92A-30	3.0
lizardite	88-B6	1050*
lizardite	88-51	700*
lizardite-skarn	92A-46	1140
malachite-skarn	93A-88	8.0
malachite-skarn	92A-33E	190
pargasite	92A-14	50*
phlogopite	92A-1C	12.5
quartz-sill	92A-36	2.5
talc	92A-6	3.3
talc	92A-7A	3.5
tremolite	92A-12	8.6
tremolite	93A-16	10.0
tremolite	93A-69B	14.0
tremolite	93A-79	6.0

* Maximum boron concentration estimated via semi-quantitative alpha-track mapping.

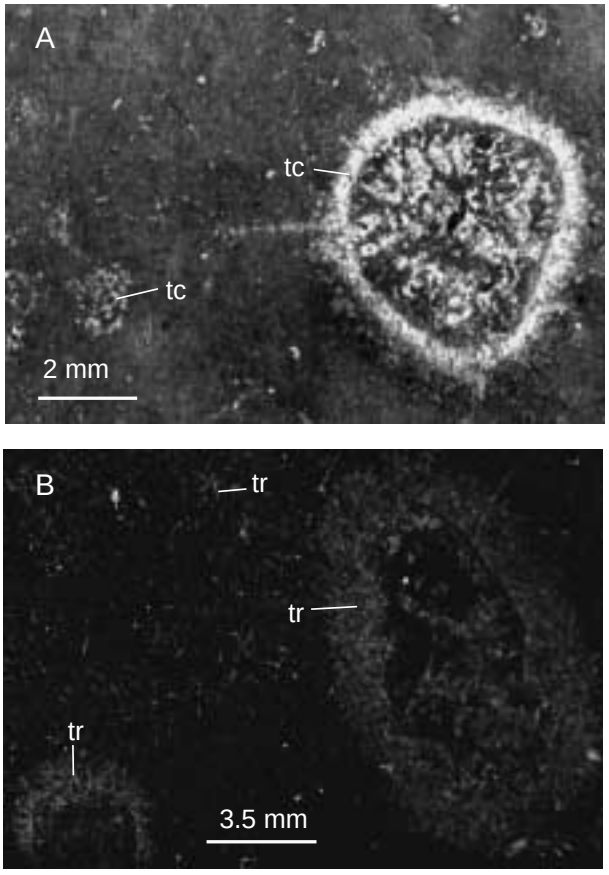

FIGURE 8. Alpha-track maps of talc- and tremolite-zone rocks. **(a)** Talc zone (88-70). Talc is found in reaction rims surrounding chert nodules. Track concentrations are associated with talc, which contains 3 ppm B. **(b)** Tremolite zone (92A-11). Tremolite is found in reaction rims surrounding chert where it replaced talc, or it is found as fibrous laths within the rock matrix. Track concentrations are associated with tremolite, which contains from 3–14 ppm B depending on sample location relative to the stock and to structural features that channeled fluids. (tc = talc; tr = tremolite).

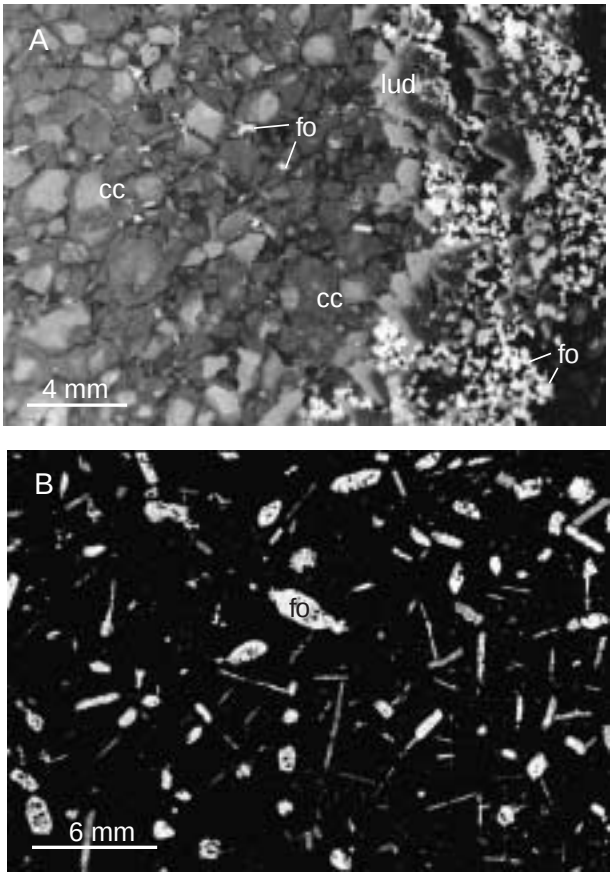

FIGURE 9. Alpha-track maps of forsterite-zone rocks. **(a)** Sample (92A-32) located about 50 m from the stock, contains both metamorphic and metasomatic forsterite. Metasomatic forsterite occurs with ludwigite in the vein along the right side of the image, and is identified by its short prismatic habit and high modal abundance. Metamorphic forsterite forms after tremolite; it is seen in the rock matrix and is identified by its elongate habit and sparse distribution. Forsterite from the vein contains 1370 ppm B. Ludwigite does not image well due to the extreme number of tracks produced, which damages the detector film. Matrix calcite shows interesting track zonation and contains an average 12 ppm B. **(b)** Sample (92A-64) located 500 m from the stock. It contains metamorphic forsterite that hosts 100 ppm B. Calcite, dolomite, spinel, sulfides, and phlogopite also are present in the sample but do not contain enough B to be imaged. (fo = forsterite; cc = calcite; lud = ludwigite).

tain relatively high B (Fig. 9a). Metasomatic forsterite generally has higher but more variable Fe concentrations than does metamorphic forsterite. Other important chemical differences include higher SiO_2 contents for metamorphic forsterite and higher MnO, CaO, B, and F contents for metasomatic forsterite. Figure 9b shows both inter- and intra-grain B variations in a forsterite-zone marble collected ~500 m from the stock. Accessory phlogopite and pargasite contain negligible B. In general, forsterite B concentrations are greater near the stock where metasomatic forsterite is abundant. Overall, the pattern of B enrichment in forsterite is not systematic, as some metasomatic forsterite contains almost no B and some proximal metamorphic forsterite contains less B than distal metamorphic forsterite.

Forsterite from the Alta aureole contains between 102 and 1374 ppm B (or 0.035–0.440 wt% B_2O_3; Table 3). In skarns from other localities, B substitution in metamorphic forsterite occurs as $B(F,OH)Si_{-1}O_{-1}$ and can reach levels up to 1.3 wt% B_2O_3 (Grew 1988, 1996; Grew et al. 1991, 1999; Sykes et al. 1994). This substitution is plausible for Alta forsterite as there is a positive correlation between F and B and a negative correlation between Si and B (Woodford 1995).

In the presence of dolomite, forsterite reacts to form clinohumite with increasing temperature. In the southern Alta aureole, the clinohumite isograd is poorly defined. Figures 10a, 10c, and 10d show alpha-tracks associated with clinohumite. Clinohumite from sample 93A-35F contains 1150 ppm B, and likely is metasomatic due to its euhedral nature and association with metasomatic ludwigite, forsterite, and spinel. In contrast, anhedral clinohumite from sample 92A-66 formed after

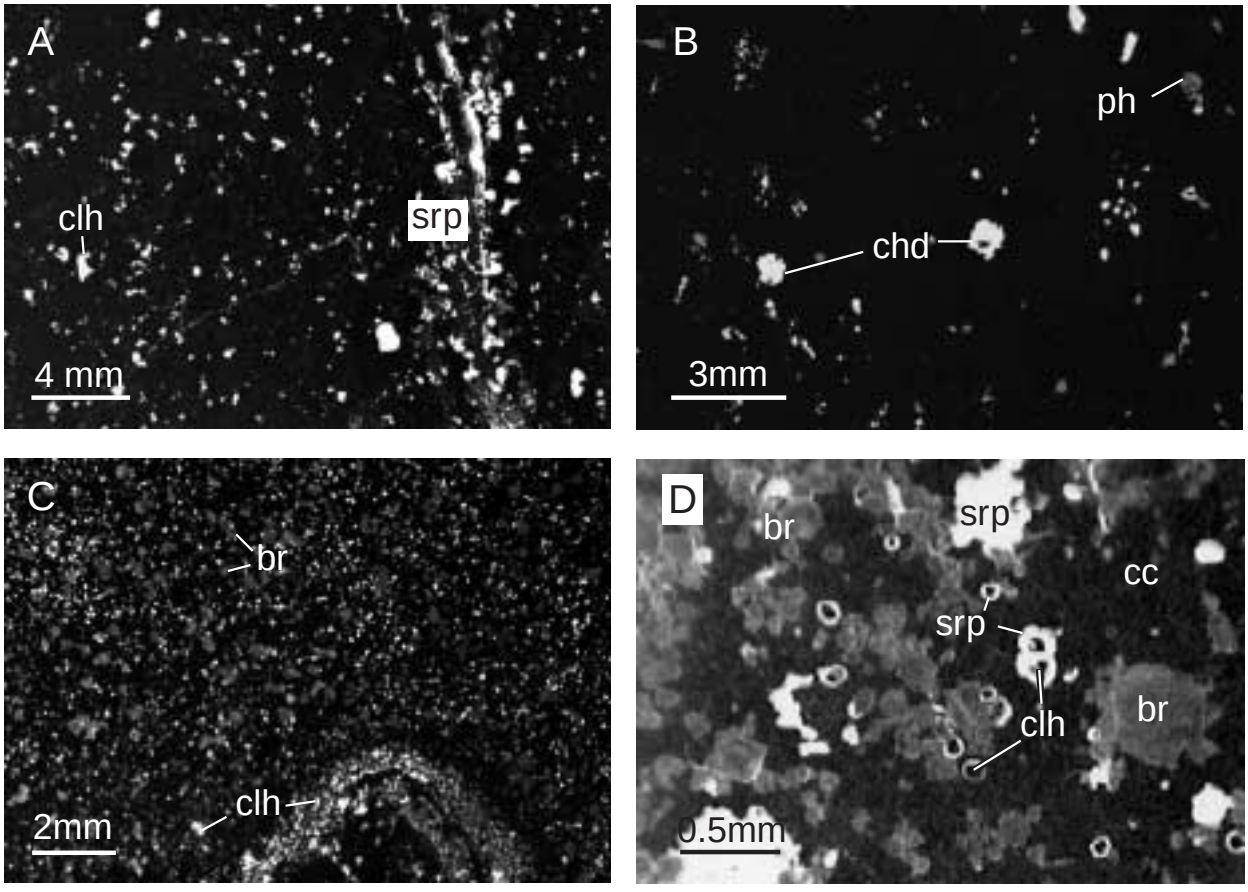

FIGURE 10. Alpha-track maps of clinohumite- and periclase-zone samples. **(a)** Clinohumite-bearing (88-B6). Serpentine has replaced clinohumite in and around the vein; both minerals contain several hundred ppm B. **(b)** Chondrodite-bearing marble (88-59). High track concentrations are due to B in chondrodite. Phlogopite may also host some B. **(c)** Clinohumite-bearing (88-40). Small bright spots are due to B in clinohumite. Brucite is seen as slightly larger grains and also contains some B. The calcite matrix hosts no B. **(d)** Clinohumite-bearing (88-51) showing low-B clinohumite replaced by high-B serpentine. Moderate track concentrations are due to brucite. Although a B-rich fluid phase circulated through this rock, B did not diffuse into the clinohumite. (clh = clinohumite; chd = chondrodite; srp = serpentine; ph = phlogopite; br = brucite; cc = calcite).

forsterite and only contains 25 ppm B, despite the fact that ludwigite also is present; textural relationships indicate that clinohumite formed before ludwigite.

Rarely, chondrodite forms instead of forsterite (Fig. 10b). Chondrodite-bearing samples contain phlogopite and have elevated whole-rock concentrations of Fe, Si, Al, Ti, and K, which suggests a metasomatic fluid influx. Boron incorporation in clinohumite and chondrodite likely occurs via the same coupled substitution of $B(F,OH)Si_{-1}O_{-1}$ as in forsterite (cf., Hinthorne and Ribbe 1974).

Brucite hosts relatively small amounts of B (Figs. 10c and 10d). For example, large (~3 mm) "onion skin" brucite masses (sample 93A-40) contain 7 ppm B. No other brucite samples were analyzed due to their small grain size and difficulty of separating a pure phase.

Skarn rocks and minerals

Three skarn types were investigated during the course of this study. These include: zoned skarn containing borate minerals around a granitic sill; zoned skarn without borate minerals around a granitic sill; and kotoite-bearing fissure skarn.

Zoned borate skarns have up to four distinct mineralogical layers (Fig. 11). Sample series 92A-33A-G is a representative example. The innermost zone (sample 92A-33G) has diopsidic pyroxene and grossular-rich garnet in a 5–8 cm thick layer adjacent to the granitic sill. In this zone, B is heterogeneously distributed in diopside whereas garnet is nearly B-free (Fig. 12a). The next skarn zone (sample 92A-33E) is 30–50 cm thick and contains magnetite, spinel, forsterite, and malachite. Magnetite and spinel do not host B (Fig. 12b). Forsterite (Fo_{95}) contains 630 ppm B and malachite contains 190 ppm B. Rare relict ludwigite grains in this zone formed early and were replaced extensively by magnetite. Also within this zone are relict pods of ludwigite- and forsterite-bearing marble. Distal to the magnetite zone is a 15 to 20 cm thick zone containing diopsidic pyroxene, clintonite, and other silicates (sample 92A-33D). Diopside and clintonite separates contain 51 and 43 ppm B, respectively, whereas the whole-rock sample contains 77 ppm

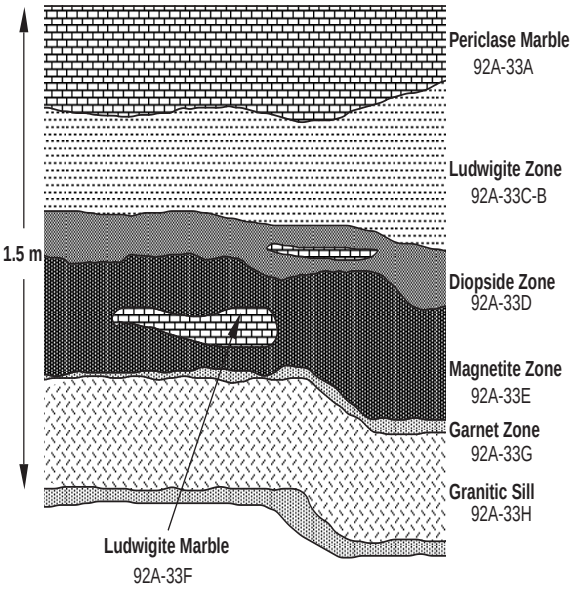

FIGURE 11. Schematic diagram of skarn sample suite 92A-33A-H. Zone H represents a granitic sill injected into periclase marble (zone A). Zone G consists of grossular-andradite series garnet and diopside. Zone E is magnetite-rich with lesser amounts of spinel, forsterite, malachite, other undetermined silicates, and relict ludwigite. Zone F is a calcite-ludwigite pod within the magnetite. Zone D contains diopside and clintonite. Zones C and B are ludwigite- and forsterite-bearing marbles with a higher concentration of ludwigite in Zone C. Boron enrichment occurs in all skarn zones and in the igneous sill, which shows fluid alteration effects (Fig. 6B).

B. Several crosscutting veins (<0.5 mm) have very high alpha-track densities (Fig. 12c), suggesting B concentrations greatly exceeding 100 ppm. A large euhedral diopside crystal from a similar skarn (sample 92A-1) displays strong oscillatory alpha-track zoning (Fig. 12d), although these zones do not coincide with major element variations (which are slight). High Al_2O_3 and low Na_2O content in this diopside suggest that Li may be present as a spodumene ($LiAlSi_2O_6$) component. Ludwigite-rich marble (sample 92A-33B-C) forms a 30–60 cm thick outermost zone containing 25–100% ludwigite and up to 10% forsterite (Fig. 13a). Calculations based on modal abundances of ludwigite, forsterite, and calcite indicate that this zone cannot be derived solely from a dolostone precursor and B-rich fluid; a substantial addition (2–4 fold enrichment) of metasomatic Mg is required. Beyond the ludwigite zone, the rock type is typically periclase marble (sample 92A-33A) with a B concentration of 24 ppm. The whole-rock MgO content of this sample (28.5 wt%) is elevated compared to tremolite, talc, and unmetamorphosed dolostones (25 wt%), and seemingly requires metasomatic addition of Mg.

The zoned nature of a small non-borate skarn (sample 92A-46A) associated with an evolved igneous sill indicates that fluids from the sill infiltrated the dolostones. The zones include: (1) wollastonite + anorthite (2 cm) adjacent to the sill, (2) garnet (0.5 cm), (3) diopside (1 cm), (4) phlogopite (0.2 cm), and (5) lizardite (1 cm) replacing forsterite. Overall, FeO decreases away from the sill. Figure 13b shows the entire skarn and adjacent sill. The sill contains 50 ppm B hosted by altered plagioclase. Boron in the wollastonite + anorthite zone (14 ppm) is primarily hosted by wollastonite. The garnet zone contains no B except for small patches where garnet is altered. The pyroxene zone hosts considerably more B (67 ppm). The phlogopite zone is B-poor, and the lizardite zone contains 1140 ppm B. Rare unaltered grains of metasomatic forsterite have low B concentrations suggesting that a later, B-rich fluid altered the forsterite to serpentine.

The third skarn (sample 92A-61) studied is a vertical fissure skarn located ~150 m from the stock/aureole contact. The main skarn exposure (0.5×4 m) consists of a mixture of grossular and diopside perpendicular to bedding. Sub-horizontal stringers of ludwigite and kotoite branch off the main skarn body parallel to bedding surfaces for about a meter. The stringers are weakly zoned with the exterior consisting of pure recrystallized calcite. Inside this zone is a kotoite-bearing marble, similar to that found at other localities (e.g., Watanabe 1963, 1967). The innermost zone contains only kotoite and ludwigite. Here, individual kotoite crystals are up to 1 cm across. The inner zone also has szaibelyite [$MgBO_2(OH)$] in millimeter-scale veins that crosscut both ludwigite and kotoite.

DISCUSSION

Borate mineralization

The general conditions of kotoite formation are known from various field and experimental studies (Barsukov and Egorov 1957; Barsukov and Deryugina 1960; Shabynin 1962; Watanabe 1967; Grigor and Brovkin 1970; Aleksandrov 1974, 1975). Watanabe (1967) hypothesized that at the Hol Kol contact deposit in North Korea, B was introduced by volatile exsolution during granite crystallization — similar to the situation at Alta. Reaction of this fluid with dolomite produced kotoite-bearing marble. If the dolomite or the fluids contain Fe, then ludwigite forms instead of kotoite (Barsukov and Egorov 1957). Watanabe (1967) proposed that the following reaction produced kotoite:

$$3 \text{ dolomite} + 2\ B(OH)_{3\ aq} = \text{kotoite} + 3 \text{ calcite} + 3\ CO_2 + 3\ H_2O.$$

Barsukov and Deryugina (1960) experimentally confirmed this reaction at 400 °C for alkaline B-bearing solutions.

Pure kotoite-bearing marble derived from pure dolostone, should have a composition of kotoite + 3 calcite, as inferred for the kotoite-bearing marble from Hol Kol. The kotoite-bearing marble at Alta also appears to have formed via the above reaction, although, the kotoite to calcite ratio is too high for the kotoite to be derived simply from the host dolostone. Mg may have been introduced metasomatically along with B as:

$$\text{dolomite} + 2\ Mg(OH)^{+}_{aq} + 2\ B(OH)^{-}_{4aq} = \text{kotoite} + \text{calcite} + CO_2 + 5\ H_2O.$$

In addition, the metasomatic enrichment of Mg resulted in much larger kotoite crystals and monomineralic kotoite rocks.

Ludwigite occurs both in skarns and disseminated along

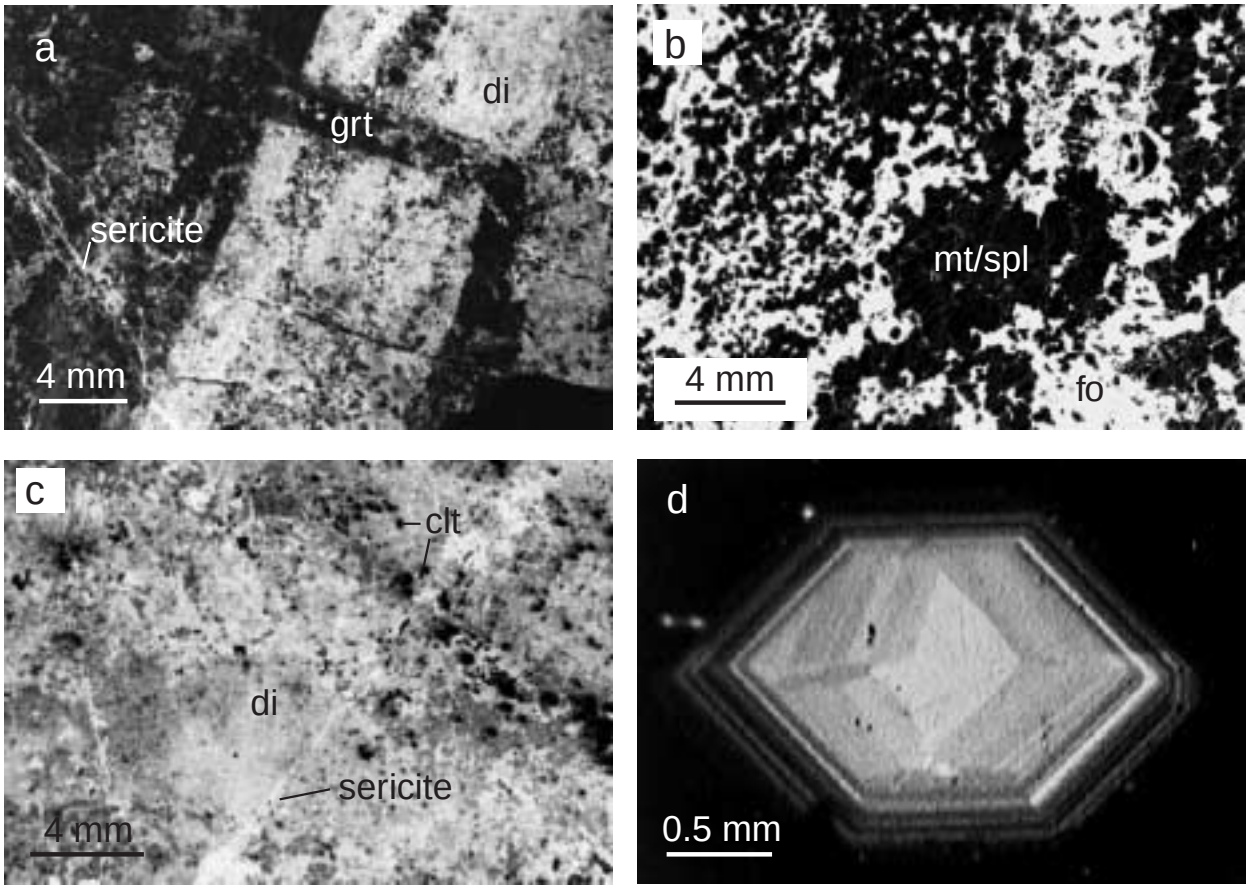

FIGURE 12. (a) Garnet-diopside skarn zone (92A-33G). High track concentrations are associated with diopside and alteration material. Garnet contains little or no B. **(b)** Magnetite skarn zone (92A-33E). High track concentrations are associated mainly with calc-silicate gangue material (especially forsterite) and minor malachite. Track-free areas correspond to magnetite and Mg-Al spinel. **(c)** ATM of the diopside-clintonite zone (92A-33D). High track concentrations are associated with diopside alteration as seen along the veins. Moderate track densities are due to diopside. Lithium is suspected in the diopside and may be responsible for some of the tracks. Lower track densities are associated with clintonite, which hosts 43 ppm B. **(d)** Oscillatory zoning in a diopside crystal cut perpendicular to the B-axis; a bulk separate of this diopside contains 43 ppm B. (di = diopside; grt = garnet; clt = clintonite; mt = magnetite; spl = spinel; fo = forsterite).

bedding planes throughout periclase-zone dolostones. Cook and Bowman (2000) noted an increase in abundance of ludwigite in the dolostone approaching the skarns. Relict pods of ludwigite and forsterite in borate skarns indicate that the skarn zones migrated outward during fluid infiltration. Textural relationships indicate that ludwigite formed after kotoite in the fissure skarn; similar textures have been observed in skarns of the Onca de Fier region, Romania (Codarcea et al. 1959; Marincea 1999, 2000) and the Brooks Hill marble, Alaska (Aleksandrov 1975).

There are distinct compositional differences between ludwigite associated with contact skarns and those within periclase-zone dolostones (Fig. 14; Table 4). In general, skarn-hosted ludwigite has a higher vonsenite component (high Fe, with low Mg, Al, and Ti), whereas dolostone-hosted ludwigite is closer to the ludwigite end-member (high Mg, Al, and Ti, with low Fe). The Fe/(Fe + Mg) ratio ranges from 0.32 to 0.36 for skarn ludwigite and is only 0.24 to 0.28 for disseminated ludwigite. Pertsev (1971) reports an association of relatively Mg-rich ludwigite with kotoite; this is not the case for ludwigite associated with kotoite at Alta (Table 4). According to Pertsev (1971), the Fe^{2+}/Mg ratio increases with silica activity; this relationship can explain the observed compositional differences at Alta as, presumably, the skarn-forming fluids had higher Si activity than those which infiltrated the dolostones. Another possible explanation for the different compositional relations at Alta is that increasing Fe^{2+} corresponds to lower ludwigite formation temperature (Kravchuk 1966). Barrese et al. (1995) reported that ludwigite forms from kotoite above 600 °C and 50 MPa. Thus, as both this reaction and periclase-zone metamorphism occur at similar temperatures, a model of different fluid compositions in the skarn and in the contact aureole seems to be the most plausible explanation.

Because szaibelyite crosscuts both ludwigite and kotoite, clearly it formed from a separate fluid pulse after kotoite and ludwigite formation. This inference is consistent with experimental constraints for formation of szaibelyite at low tempera-

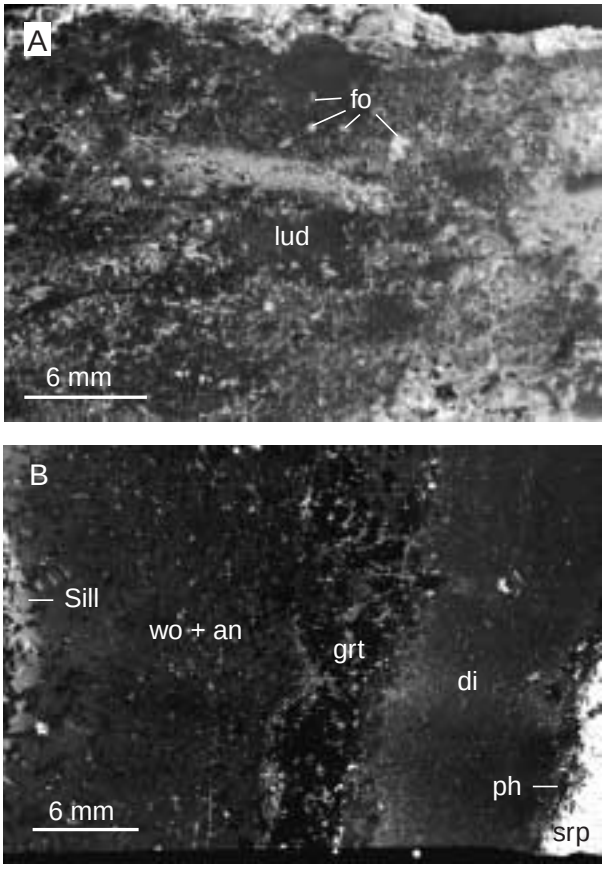

FIGURE 13. (a) Alpha-track map of the ludwigite skarn zone (92A-33B). Ludwigite does not image well on ATMs due to its extremely high track density. Forsterite is common in this zone and hosts a considerable amount of B. Calcite contains only small amounts of B. **(b)** Composite skarn (92A-46B) showing small-scale mineral zonation. Igneous sill material is seen on the left side. Skarn zones include wollastonite-anorthite, garnet, diopside, phlogopite, and lizardite after forsterite. (lud = ludwigite; fo = forsterite; wo = wollastonite; an = anorthite; grt = garnet; di = diopside; ph = phlogopite; srp = serpentine).

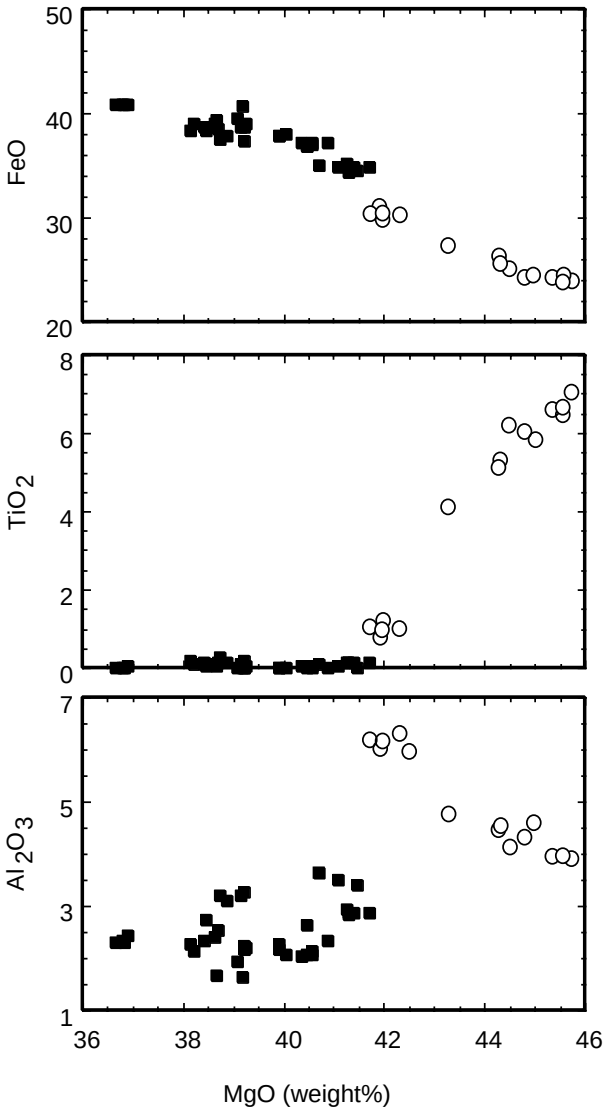

FIGURE 14. FeO, TiO_2, Al_2O_3, and MgO variations in ludwigite define two distinct compositional groups. Low-Mg, high-Fe ludwigite (filled squares) is associated with contact skarn formation, whereas high-Mg, low-Fe ludwigite (open circles) occurs along carbonate beds or in veins not directly associated with skarnification. Each point represents a single analysis. Data are from Table 4 and Woodford (1995).

tures of ~250–150 °C (Barsukov and Deryugina 1960; Aleksandrov 1974).

Metasomatic effects

The geochemical data are consistent with the origin of solute-rich fluids in the stock and with lateral down-temperature flow into the country rocks. Metasomatic enrichments for most elements are resticted to within a kilometer of the stock; more extensive mass transport likely was precluded by reactivity and limited volume of fluids emanating from the pluton. The Ca/Mg ratio varies from 1.2 for unmetamorphosed and low-grade dolostones, to 6.0 for high-grade marbles. Thus, in the high-grade rocks, it appears that Mg was selectively removed by fluids. There was only limited Ca mobility in the aureole compared to Mg, as indicated by dolomite-bearing veins in talc-zone rocks (Cook 1992), the presence of Mg-rich borates, and evidence for the presence of $MgCl_2$ in skarn fluid inclusions. Due to the increased solubility of dolomite over calcite at high temperatures (Barsukov and Egorov 1957; Pankow 1991), removal of Mg from dolostone is common elsewhere in regions with Mg-borate mineralization.

Figure 7 summarizes B concentrations in igneous rocks at Alta. Because unaltered, highly evolved pegmatite and aplite dikes within the stock contain little B compared to fluid-altered highly evolved sills within the aureole, it appears that B concentrations depend more on the degree of fluid alteration

TABLE 4. Representative borate analyses

Sample	92A–19 ludwigite	93A–35F ludwigite	92A–61A ludwigite	92A–61A kotoite	92A–61C szaibelyite
SiO_2	0.12	0.09	0.12	0.52	0.36
Al_2O_3	3.51	4.53	2.26	0.02	0.04
TiO_2	0.04	5.32	0.00	0.02	0.00
FeO	2.54	0.38	4.05	0.55	1.04
Fe_2O_3	35.82	28.06	37.52	0.00	0.00
MgO	41.09	44.32	39.91	62.98	46.19
MnO	0.11	0.08	0.15	0.19	0.07
CaO	0.04	0.02	0.01	0.03	0.07
Na_2O	0.00	0.00	0.02	–	–
K_2O	0.01	0.01	0.01	–	–
SnO_2	0.05	0.01	0.00	–	–
B_2O_3	18.66	20.02	15.56	32.98	38.54
F	–	–	–	0.00	0.00
H_2O*	–	–	–	–	10.08
Total	101.99	102.84	102.61	97.29	96.39
Formula proportions based on indicated no. of O atoms					
0	5	5	5	6	3
Si	0.00	0.00	0.00	0.02	0.01
Al	0.13	0.16	0.08	0.00	0.00
Ti	0.00	0.12	0.00	0.00	0.00
Fe^{2+}	0.07	0.01	0.11	0.02	0.01
Fe^{3+}	0.85	0.64	0.90	0.00	0.00
Mg	1.93	1.99	1.89	3.11	1.01
Mn	0.00	0.00	0.00	0.01	0.00
Ca	0.00	0.00	0.00	0.00	0.00
Na	0.00	0.00	0.00	–	–
K	0.00	0.00	0.00	–	–
Sn	0.00	0.00	0.00	–	–
B	1.01	1.04	1.02	1.89	0.98
F	–	–	–	0.00	0.00
H	–	–	–	–	0.99

* H_2O calculated assuming ideal stochiometry. For ludwigite, Fe_2O_3 calculated assuming 4 atoms per formula unit.

than on the extent of igneous differentiation. These sills formed along planes of weakness, which likely served as natural conduits for channeling exsolved aqueous fluids from the stock to the aureole. However, evidence cited above also indicates that some magmatic B was lost accompanying fluid exhalation as the melts solidified.

Possible sources of boron in the contact aureole

Three distinctive reservoirs are plausible B sources for the enrichments observed in Alta marbles. The first is the unmetamorphosed or precursor dolostone that has a B concentration of < 2 ppm. As whole-rock B concentrations from marble in each metamorphic zone are equal to or greater than 2 ppm, closed-system self-sourcing scenarios are precluded. Boron mobilization from beyond the zone of thermal metamorphism also is unlikely as there is no evidence for an external heat and/or fluid source. However, Ferry (1994) suggested the possibility of lateral up-temperature fluid flow in the talc, tremolite, and forsterite zones at Alta; assuming that a single occurrence of dol + qtz + tlc + cal in the talc zone (Moore and Kerrick 1976) can be generalized throughout the *massive* dolostone, Ferry calculated an up-temperature flow of ~30 m^3 fluid/m^2 rock. However, he also stated that such isobaric univariant assemblages may be rare in the aureole. If so, then down-temperature flow may be permissible. Although this assemblage is common in *nodular* Alta dolostones (Moore and Kerrick 1976; Cook 1992), it is not considered to be in equilibrium because the formation of concentric mineral zones separates reactants and limits mass diffusion. Equilibrium univariant and invariant assemblages in *massive* Alta dolostones were not observed during this study and are poorly documented elsewhere. For these reasons, the unmetamorphosed carbonates are not considered a likely source of B enrichments.

The second source reservoir considered is the relatively B-rich (90 ppm) Ophir shale that stratigraphically underlies the marbles. It is reasonable to suppose that a vertical component of fluid movement could extract B from the shale and enrich the carbonates. However, this model is not favored for the following reasons. First, the very low permeability of the pelitic material precludes significant vertical fluid flow (Cook 1992). Field observations confirm the impermeable nature of the Ophir pelites where the intrusion of fluid-inclusion-rich pegmatitic dikes between shale layers resulted only in thermal metamorphism of the pelites, but not skarn formation or other fluid-related changes. Second, the metamorphosed shale does not appear to be depleted in B as alpha-track analysis of the Ophir shale near the contact (sample 92-36) indicates that the micas are still B-rich (Woodford 1995). Nor is a vertical gradient of decreasing B concentration observed in the carbonates with distance from the shale/marble contact, as might be expected. In fact, the opposite appears to be true as B enrichment of tremolite occurs toward the Alta-Grizzly thrust, which stratigraphically overlies the marbles. Our study does not rule out the possibility that some B was leached from the Ophir Formation by fluids moving along the contact, but mass-balance calculations indicate that this is an unlikely source for the bulk of metasomatic B in the aureole.

The third B reservoir considered is the Alta Stock. It is the most viable B source for the following reasons. (1) Borate mineralization is concentrated near the contact and is texturally related to the intrusion (i.e., the ludwigite zone in contact replacement skarns). (2) Oxygen isotopic data from marbles imply exchange with a fluid source equilibrated with the stock (Cook 1992; Cook et al. 1997). (3) Exsolved magmatic fluids, shown by John (1991) to be in oxygen isotopic equilibrium with the stock, are shown in this study to contain B. (4) Fluid inclusion studies show that skarn fluids are related to fluids from the stock or related sills. (5) The isotopic composition of aureole B is similar to that of igneous B (Woodford 1995; Woodford and Leeman unpublished data).

Fluid evolution and infiltration at Alta

The development of the Alta hydrothermal system was complex and an overall model must successfully accommodate information from all previous studies (Moore and Kerrick 1976; Cook 1982; Kemp 1985; John 1991; Cook 1992; Ferry 1991, 1994; Bowman et al. 1994; Cook and Bowman 1994, 2000; Gerdes et al. 1995; Cook et al. 1997). An overview is provided here.

As summarized by John (1991): (1) The Alta stock initially contained about 3–4 wt% H_2O, of which about 1 wt% is now incorporated in hydrous minerals. (2) Vapor saturation did not occur until a fairly late stage of crystallization, resulting in low fracture permeability in the stock relative to more H_2O-rich systems of similar composition. (3) Fluid inclusion studies indicate that vapor saturation of the magma occurred at ~720 °C.

(4) Pervasive but weak deuteric alteration of the stock by magmatic fluids resulted in sericitization of feldspar at ~500 °C. As shown in this study, the presence of B in the sericite is evidence that B partitioned into exsolved magmatic fluids. (5) Six different vein generations formed progressively from magmatic fluids as the stock cooled between 530 and 465 °C; a seventh vein generation formed at lower temperatures due to a late-stage incursion of meteoric fluids. Boron is present in minerals and selvage zones of the magmatically derived vein generations. Vein mineral compositions show that the fluids also contained Si, Fe^{3+}, Fe^{2+}, Al, K, Ca, Mg, Ti, Na, Cu, Mo, F, and Cl. The presence of Fe, Mg, K, Na, and Cl is indicated by both fluid-inclusion microthermometry and daughter minerals. It is possible that B is located in the abundant fluid inclusions occurring within the quartz, as fluid inclusions found elsewhere have high B concentrations (e.g., Bottrell and Yardley 1988; Banks and Yardley 1992).

Exsolved fluids were channeled along grain boundaries and small stockwork fractures until they reached the contact with Paleozoic carbonates. In addition, evolved residual magmas were injected as sills along carbonate bedding planes through which fluids were preferentially channeled. If the sill-forming magma also was B-enriched, viscosity may have been reduced by the effects of B-fluxing (Dingwell et al. 1992), enabling the formation of relatively thin sills at large distances (~100 m) from the contact.

Simple volumetric calculations [assuming a cylindrical geometry with a 1.3 km radius and height of 150 m (= thickness of aureole)] indicate that if all of the dissolved water (3–4 wt%) was exsolved radially, the total fluid flux at the contact would be 2.9 to 3.9×10^6 mol fluid/m^2. As this is about an order of magnitude lower than the contact flux value of 4.2×10^7 calculated by Cook and Bowman (2000), a different flow pattern is inferred for fluids within the stock. Figure 15 shows the circulation pattern determined by Cook et al. (1997) to best reproduce observed oxygen isotope and thermal profiles in the Alta aureole. Upward fluid movement within the stock and lateral dispersion near the top, requires that low permeability structures (i.e., Ophir Shale, Alta-Grizzly Thrust) forced fluids to move laterally rather than vertically within the aureole. This interpretation is supported by the observation that, within the periclase zone, brucite-rich layers (10–30 cm thick) alternate with brucite-absent dolostone layers. This pattern of occurrence is inconsistent with pervasive vertical fluid flow (Cook and Bowman 1994), and likely resulted from differences in the initial SiO_2 concentration of individual dolostone layers and consequent reaction-induced porosity and increased fluid flow along SiO_2-rich beds. Heterogeneous permeability between layers also is noted in the distal tremolite- and talc-zone rocks (Gerdes et al. 1995; Cook and Bowman 2000).

To assess whether or not the excess B in the periclase and forsterite zones could be supplied by that initially available in the Alta stock, we performed a simple mass-balance calculation. Using parameters in Table 5, we estimated that approximately 7.4×10^7 kg of B was metasomatically added to the aureole. Taking the time-integrated fluid flux of 4.2×10^7 mol fluid/m^2 (through roughly half the carbonate layers to account for permeability heterogeneity), an estimated total of 4.6×10^{11} kg of fluid infiltrated the aureole dolostones. Combined with our estimate of B added to the aureole, and assuming that 2–3 wt% (of the maximum 4% available) of magmatic H_2O exsolved from the stock, we calculated an average time-integrated aureole fluid B concentration of 160 ± 40 ppm B (Table 6). This value is within the range measured for B contents of fluid inclusions for both metamorphic and magmatic fluids (Leeman and Sisson 1996).

In addition, we approximated the average B content of exsolved magmatic fluids (and of the magma prior to crystallization) by using the magma/stock volume required to exactly balance the time-integrated fluid flux (Cook and Bowman 2000) and assuming that all fluid originated in the stock. An unknown in this calculation is the height of the stock. From the estimated amount of fluid that infiltrated the periclase zone, the maximum amount of water (2–3 wt%) derived from the magma (allowing 1% to remain in hydrous silicates), and an idealized cross-sectional area of the stock, we calculated a cylindrical volume of degassed magma with height between 1118–1678 m. Numerically recombining the approximately 7.4×10^7 kg of B in the aureole back into the equivalent mass for the outgassed portion of the stock suggests that initial magmatic B concentration could have ranged between 7–10 ppm (Table 6). This estimate includes the 4.4 ppm B now largely hosted by sericitic alteration of feldspar within the stock. These figures suggest that exhalative loss of approximately 50% of the initial magmatic B could balance that added to the aureole; this result is consistent with experimental determinations of B partitioning between aqueous vapor and granitic melts (cf., Pichavant and Manning 1984). Assuming that all B from the magma was initially partitioned into the fluid phase, and allowing for a 25% uncertainty in the estimated amount of B added to the aureole, we calculated maximum time-integrated magmatic fluid concentrations in the range of 270–420 ppm B (Table 6).

In reality, the B content of fluids likely was highly variable both spatially and temporally, as evidenced by oscillatory track zoning in diopside (Fig. 12d) and by highly variable B contents in metamorphic orthosilicates. Fluids responsible for ludwigite formation may have had significantly higher B contents. Variations in the B content of fluids and/or magma through time could result from differential fluid exsolution between crystallized regions of the magma chamber and regions containing B-rich residuals, and from fluid-mineral partitioning during progressive fluid-rock interaction.

As these B-rich fluids infiltrated the country rock, skarns formed along contacts and along structures that channeled fluids. While the exact nature of these fluids is unknown, it is reasonable to assume that their initial pH was acidic (Helgeson 1964; Guilbert and Park 1986; Skinner 1997). In reactions between acidic fluid and dolostone, carbonate consumes H^+ and the solution is effectively neutralized. This acid neutralization results in skarn formation as solute elements are precipitated. As fluid further equilibrates with carbonate, pH increases and it becomes basic (Pankow 1991). Ludwigite can only occur in alkaline media (Aleksandrov 1975), and B incorporation in ludwigite-zone calcite (~40 ppm, Fig. 9) may have been enhanced by high pH fluids (Hobbs and Reardon 1999). Thus,

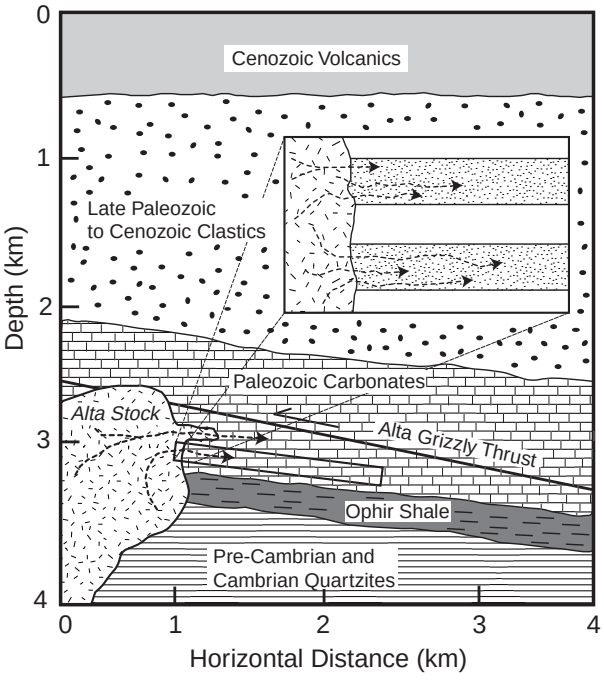

FIGURE 15. Model of stock emplacement (after Cook 1992) showing the fluid circulation pattern that best matches observed thermal and isotopic data. The dashed lines with arrows are hypothetical fluid paths from the cooling magma. The outlined region approximates the transect shown in figures 4 and 5. The inset box shows schematic infiltration of magmatic fluids into heterogeneous, relatively permeable carbonate strata of the periclase zone.

the characteristic skarn zoning from garnet-diopside to magnetite and finally ludwigite likely is due to changes in fluid pH. Although zoning could reflect changing element chemical potentials or activity gradients with changing temperature and pressure (Kwak 1987), this is probably a minor effect at Alta as temperature and pressure did not change substantially during Stage I skarn formation (Cook 1982; Kemp 1985; Bowman et al. 1985). Temperature gradients near the contact may have caused chemical changes necessary for zonation in some of the larger skarns, but for small (<100 cm) skarns associated with sill emplacement, it is unlikely that significant temperature gradients existed. Such gradients would have caused thin sills to lose heat quickly to the surrounding country rock and solidify, thus precluding emplacement beyond a few meters.

A range of fluid chemical compositions existed as documented by differences in mineral assemblages at each skarn locality as well as by variations in ludwigite chemistry (Fig. 14, Table 4). In addition, a wide range in homogenization temperature for skarn and sill fluid inclusions (Fig. 3) indicates that fluid infiltration occurred in episodic pulses. For example, the kotoite skarn had at least three such episodes in one location. The first Mg-rich and Fe-poor fluid pulse produced kotoite. A second fluid pulse introduced Fe and reacted with kotoite to form ludwigite. A third alkaline fluid pulse resulted in the formation of szaibelyite during cooling.

Other examples of temporal fluid variations are found in non-skarn ludwigite-bearing rocks in the periclase zone. In ludwigite-bearing dolostones, brucite is noticeably absent, but present in adjacent layers that do not contain ludwigite. Furthermore, modal mineral distributions indicate that Si, Fe, and Al were introduced metasomatically. Magnesium also was

TABLE 5. Aureole boron mass balance

Lithology	Inner radius (m)	Outer radius (m)	Volume‡ (m^3)	Density (kg/m^3)	avg. B (ppm)§	∑B (kg)
Periclase zone	1300	1500	2.64E+08	2700	23	1.64E+07
Forsterite zone	1500	2050	9.20E+08	2700	16	3.97E+07
Skarns*			2.59E+07	3000	250	1.94E+07
Ludwigite marble†			5.28E+05	3000	10000	1.58E+07
Estimated total B added to aureole = 7.39E+07‖						

* Skarns are assumed to comprise 1% of the periclase zone.
† Ludwigite marble is assumed to comprise 20% of the skarn.
‡ A vertical thickness of 150 m and annular form are assumed.
§ Average B content for each rock unit.
‖ Conservative estimate of uncertainity is on the order of at least ± 25%.

TABLE 6. Time-integrated average boron content of fluids and magma

Excess B Alta aureole (cf. Table 5)	5.54 x 10^7 kg B added		7.39 x 10^7 kg B added		9.24 x 10^7 kg B added	
Assumed magmatic fluid exsolved	2% H_2O*	3% H_2O†	2% H_2O	3% H_2O	2% H_2O	3% H_2O
Average aureole fluid (ppm B)‡	120	120	160	160	200	200
Average stock fluid (ppm B)§	340	266	380	306	420	346
Initial magma composition (ppm B)‖	6.8	8.0	7.6	9.2	8.4	10.4
Percent of magmatic B exsolved #	35	45	42	52	48	58

Note: These calculations assume 4.2×10^7 mol/m^2 time integrated fluid flux (Cook and Bowman 2000) with fluid flow concentrated into half of the carbonate layers. Three sets of calculations are presented to reflect ±25% uncertainty in the estimated B addition to the Alta aureole.
* Requires fluid released from a cylindrical stock with a height of 1678 m.
† Requires fluid released from a cylindrical stock with a height of 1118 m.
‡ Calculated as (excess aureole B)/(total fluid mass).
§ Calculated as estimated (total magmatic B)/(total fluid mass); assumes all B was mobilized.
‖ Calculated as (excess aureole B + total pluton B)/(mass of pluton needed to provide total fluid flux).
Fraction of estimated magmatic B lost relative to that retained (avg. = 4.4 ppm) in the Alta stock.

mobile as indicated by the heterogeneous distribution of orthosilicates, ludwigite, and spinel and by the presence of secondary dolomite. Textural relations among spinel, ludwigite, and orthosilicates indicate that spinel formed first, ludwigite second, and subsequently clinohumite and forsterite. The formation of ludwigite requires an Fe^{3+}-rich fluid as there is little Fe in the unmetamorphosed dolostone. A possible scenario involves the infiltration of a Fe-bearing, B-rich fluid that removes CO_2 and allows periclase to form. Next, periclase reacts with the Fe and B in solution to form ludwigite. A second pulse or further infiltration of fluid containing Mg, Si, and F leads to the reaction of periclase to form clinohumite. A drop in the F content of the fluid or infiltration of a distinct, low-F fluid pulse allows forsterite to form by reaction of periclase with Si. It also is possible that fluids, rather than (or in addition to) periclase, provided the necessary Mg for the formation of spinel, ludwigite, and metasomatic orthosilicates. Evidence for this process is found in (1) ludwigite veins (which also contain spinel and forsterite), (2) the presence of $MgCl_2$ in skarn fluid inclusions, and (3) ludwigite border zones surrounding contact skarns, which contain more Mg than the parent dolostone. Thus, Mg either was mobilized within the carbonates, was present in exsolved magmatic fluids, or both.

Temporal relationships between different pulses of magmatic fluids remain problematic, but some generalizations are possible. Early fluids to infiltrate the carbonates were those associated with contact skarn formation (stage 1) and/or the emplacement of aureole sills. These contained abundant Al, Si, Fe, and B, and were highly reactive due to a lower initial pH and/or a higher initial temperature. Compositional variations existed, as evidenced by the fact that skarns associated with more-evolved sills tend to lack Fe, Al, or Si mineralization. The formation of non-skarn ludwigite and metasomatic forsterite disseminated along carbonate beds near the stock represents a later fluid phase. Ludwigite compositions indicate that these fluids were more highly oxidized than stage I skarn fluids and contained very little Fe^{2+}. This inference is consistent with an increase in the oxidation state of the stock during crystallization (John 1991). It appears that this fluid phase was less reactive due to a higher initial pH, lower temperature, or both. Element concentrations (including B) were variable, as some carbonate layers contain only a few ludwigite grains whereas the mineral is abundant in others. After skarn and borate formation, equilibrated alkaline fluids migrated along permeable dolostone beds within the aureole. The fluids were depleted in elements such as Fe, Si, Al, and B relative to their original magmatic compositions. Lower B activity may have precluded further borate mineralization; rather, B was taken up at trace levels in a variety of calcsilicate minerals. Orthosilicates were particularly good recorders of B metasomatism (Grew et al. 1991) and indicate that these fluids infiltrated more than 500 m from the stock.

ACKNOWLEDGMENTS

We thank John Bowman and David John for providing additional samples as well as helpful advice. John Bowman kindly permitted us to use unpublished trace element data for samples described by Cook and Bowman (2000). Steve Cook, Ulrich Petersen, George Harlow, Martha Gerdes, and Milton Pierson all contributed valuable assistance in several aspects of this study. Funding was provided by GSA Research Grants, Sigma Xi Grants in Aid of Research, and NSF grants EAR90-18996, EAR90-14802, and EAR91-19110. We highly appreciate the thoughtful reviews by Edward Grew, Natalie Marchildon, and Peter Nabelek.

REFERENCES CITED

Aleksandrov, S.M. (1974) A laboratory study of the occurrence of kotoite in the MgO-B_2O_3-H_2O-CO_2 system. Geochemistry International, 11, 1336.

———(1975) Geochemical aspects of B-Sn ore formation in Alaska deposits. Geochemistry International, 12, 139–150.

Baker, A.A., Calkins, F.C., Crittenden, M.D., and Bromfield, C.S. (1966) Geologic map of the Brighton quadrangle, Utah. U.S. Geological Survey, Map GQ–534.

Banks, D.A. and Yardley, B.W.D. (1992) Crush-leach analysis of fluid inclusions in small natural and synthetic samples. Geochimica et Cosmochimica Acta, 56, 245–248.

Barrese, E., Bellezza, M., and Flamini, A. (1995) Synthesis of ludwigite. Neus Jahrbuch für Mineralogie, Monaschefte, 1995 (2), 49–55

Barsukov, V.L. and Deryugina, N.N. (1960) An experimental investigation of the conditions of formation of kotoite-asharite ores. Geokhimiya, no. 1, 66–71.

Barsukov, V.L. and Egorov, A.P. (1957) Some geochemical characteristics of conditions of formation of hypogene borate deposits. Geokhimiya, no. 8, 790–801.

Barton, M.D., Ilchik, R.P., and Marikos, M.A. (1991) Metasomatism. Mineralogical Society of America, Reviews in Mineralogy, 26, 321–350.

Bebout, G.E. and Carlson, W.D. (1986) Fluid evolution and transport during metamorphism: evidence from the Llano uplift, Texas. Contributions to Mineralogy and Petrology, 92, 518–529.

Bottrell, S.H. and Yardley, B.W.D. (1988) The composition of a primary granite-derived ore fluid from S.W. England, determined by fluid inclusion analysis. Geochimica et Cosmochimica Acta, 52, 585–588.

Bowers, T.S. and Helgeson, H.C. (1983) Calculation of the thermodynamic and geochemical consequences of non-ideal mixing in the system H_2O-CO_2-NaCl on phase relations in geologic systems: Equations of state for H_2O-CO_2-NaCl fluids at high pressures and temperatures. Geochimica et Cosmochimica Acta, 47, 1247–1275.

Bowman, J.R. (1986) Groundwater influx coupled with the transition from lithostatic to hydrostatic fluid pressure during contact skarn development. EOS, Transactions of the American Geophysical Union, 67 (16), 272.

Bowman, J.R. and Essene, E.J. (1982) P-T-XCO_2 conditions of contact metamorphism in the Black Butte aureole, Elkhorn, Montana. American Journal of Science, 282, 311–340.

Bowman, J.R., Connelly, M.P., Cook, S.J., and Covert, J.J. (1985) Changes in temperature, fluid sources, and fluid pressure relative to total pressure during contact skarn development. EOS, Transactions of the American Geophysical Union, 66, 1143.

Bowman, J.R., Willett, S.D., and Cook, S.J. (1994) Oxygen isotopic transport and exchange during fluid flow: One-dimensional models and applications. American Journal of Science, 294, 1–55.

Codarcea, A., Kissling, A., and Kissling, M. (1959) Asupra ludwigitului de la Onca de Fier. Academia Romana Buletin Stiintific Sectiunea Geologie si Geografie, 2, 515–527 (in Romanian).

Cook, S.J. (1982) The physical-chemical conditions of contact skarn formation at Alta, Utah. Master's thesis, University of Utah, 169 p.

———(1992) Contact metamorphism surrounding the Alta Stock, Little Cottonwood Canyon, Utah. Ph.D. dissertation, University of Utah, 216 p.

Cook, S.J. and Bowman, J.R. (1994) Contact metamorphism surrounding the Alta Stock: thermal constraints and evidence of advective heat transport from calcite + dolomite geothermometry. American Mineralogist, 79, 513–525.

———(2000) Mineralogical evidence for fluid-rock interaction accompanying prograde contact metamorphism of siliceous dolomites: Alta Stock Aureole, Utah, USA. Journal of Petrology, 41, 739–757.

Cook, S.J., Bowman, J.R., and Forster, C.B. (1997) Contact metamorphism surrounding the Alta stock: Finite element model simulation of heat and O^{18}/O^{16} mass-transport during prograde metamorphism. American Journal of Science, 297, 1–55.

Cranor, J.I. (1974) Petrology and geochemistry of the calc-silicate zone adjacent to the Alta and Clayton Peak Stocks near Brighton, Utah. Brigham Young University Geological Studies, 21, 151–176.

Crittenden Jr., M.D. (1965) Geology of the Dromedary Peak quadrangle, Utah. U.S. Geological Survey Map GQ-378, 1 sheet.

Dingwell, D.B., Knocke, R., Webb, S.L., and Pichavant, M. (1992) The effect of B_2O_3 on the viscosity of haplogranitic liquids. American Mineralogist, 77, 457–461.

Dipple, G.M. (1998) Reactive dispersion of stable isotopes by mineral reaction during metamorphism. Geochimica et Cosmochimica Acta, 62, 3745–3757.

Farmer, G.L. and DePaolo, D.J. (1983) Origin of Mesozoic and Tertiary granite in the Western United States and Implications for Pre-Mesozoic Crustal Structure 1. Nd and Sr isotopic studies in the geocline of the northern Great Basin. Journal of Geophysical Research, 88, 3379–3401.

Ferry, J.M. (1986) Reaction progress: a monitor of fluid-rock interactions during

metamorphic and hydrothermal events. Advances in Physical Geochemistry, 5, 60–88.
———(1989) Contact metamorphism of roof pendants at Hope Valley, Alpine County, California, USA. Contributions to Mineralogy and Petrology, 101, 402–417.
———(1991) Dehydration and decarbonation reactions as a record of fluid infiltration. Mineralogical Society of America, Reviews in Mineralogy, 26, 351–391.
———(1994) Role of fluid flow in the contact metamorphism of siliceous dolomitic limestones. American Mineralogist, 79, 719–736.
———(1995) Role of fluid flow in the contact metamorphism of siliceous dolomitic limestones—Reply. American Mineralogist, 80, 1226–1228.
Ferry, J.M. and Gerdes, M.L. (1998) Chemically reactive fluid flow during metamorphism. Annual Reviews of Earth and Planetary Sciences, 26, 255–288.
Gerdes, M.L., Baumgartner, L.P. and Person, M. (1995) Stochastic permeability models of fluid flow during contact metamorphism. Geology, 23, 945–948.
Grant, S.K. (1966) Metallization and paragenesis in the Park City district, Utah. Ph.D. dissertation, University of Utah.
Grew, E.S. (1988) Kornerupine at the Sar-e-Sang, Afghanistan, whiteschist locality: Implications for tourmaline-kornerupine distribution in metamorphic rocks. American Mineralogist, 73, 345–357.
——— (1996) Borosilicates (exclusive of tourmaline) and boron in rock-forming minerals in metamorphic environments. Mineralogical Society of America, Reviews in Mineralogy, 33, 387–502.
Grew, E.S., Pertsev, N.N., Boronikhin, V.A., Borisovskiy, S.Y., Yates, M.G. and Marquez, N. (1991) Serendibite in the Tayozhnoye deposit of the Aldan Shield eastern Siberia, U.S.S.R. American Mineralogist, 76, 1061–1080.
Grew, E.S., Yates, M.G., Adams, P.M., Kirkby, R., and Wiedenbeck, M. (1999) Harkerite and associated minerals in marble and skarn from Crestmore quarry, Riverside County, California and Cascade Slide, Adirondack Mountains, New York. Canadian Mineralogist, 37, 277–296.
Grigor, Y.A.P. and Brovkin, A.A. (1970) A study of the binary section sellaite-kotoite in the MgO-MgF_2-B_2O_3 system. Doklady Akademii Nauk SSSR, 186, 1387–1390.
Guilbert, J.M. and Park, Jr. C.F. (1986) The Geology of Ore Deposits. W.H. Freeman and Company, New York. 985 p.
Hanson, R.B. (1992) Effects of fluid production on fluid flow during regional and contact metamorphism. Journal of Metamorphic Geology, 10, 87–97.
———(1995a) The hydrodynamics of contact metamorphism. Geological Society of America Bulletin, 107, 595–611.
———(1995b) Role of fluid flow in the contact metamorphism of siliceous dolomitic limestones—Discussion. American Mineralogist, 80, 1222–1225.
Helgeson, H.C. (1964) Complexing and Hydrothermal Ore Deposition, 128 p. Macmillan, New York.
Hinthorne, J.R. and Ribbe, P.H. (1974) Determination of boron in chondrodite by ion microprobe analysis. American Mineralogist, 59, 1123–1126.
Hobbs, M.Y. and Reardon, E.J. (1999) Effect of pH on boron co-precipitation by calcite: Further evidence for non-equilibrium partitioning of trace elements. Geochimica et Cosmochimica Acta, 63, 1013–1021.
John, D.A. (1989) Geologic setting, depths of emplacement, and regional distribution of fluid inclusions in intrusions of the central Wasatch Mountains, Utah. Economic Geology, 84, 386–409.
———(1991) Evolution of hydrothermal fluids in the Alta stock, central Wasatch mountains, Utah. U.S. Geological Survey Bulletin, 1977, 51 p.
Kemp, III W.M. (1985) A stable isotope and fluid inclusion study of the contact Al(Fe)-Ca-Mg-Si skarns in the Alta Stock aureole, Alta, Utah. Master's thesis, University of Utah, USA, 65 p.
Kravchuk, T.A., Nerasov, I.Y., and Grigoriev, A.P. (1966) Mineral formation conditions of the ludwigite-vonsenite series, according to experimental data. Zap Vses Mineralog Obshchestva, 95 (3), 272–286 (in Russian).
Kwak, T.A.P. (1987) W-Sn Skarn Deposits and Related Metamorphic Skarns and Granitoids, 451 p. Elsevier, New York.
Leeman, W.P. and Sisson, V.B. (1996) Geochemistry of boron and its implications for crustal and mantle processes. Mineralogical Society of America, Reviews in Mineralogy, 33, 645–707.
Marchildon, N. and Dipple, G.M. (1998) Irregular isograds, reaction instabilities, and the evolution of permeability during metamorphism. Geology, 26, 15–18.
Marincea, S. (1999) Ludwigite from the type locality, Ocna de Fier, Romania: New data and review. Canadian Mineralogist, 37, 1343–1362.
———(2000) The influence of Al on the physical and crystallographic properties of ludwigite in three Romanian occurrences. European Journal of Mineralogy, 12, 809–823.
McGee, J.J. and Anovitz, L.M. (1996) Electron probe microanalysis of geologic materials for boron. Mineralogical Society of America, Reviews in Mineralogy, 33, 771–788.
Moore, J.N. and Kerrick, D.M. (1976) Equilibria in siliceous dolomites of the Alta aureole, Utah. American Journal of Science, 276, 502–524.
Nabelek, P.I. and Labotka, T.C. (1993) Implications of geochemical fronts in the Notch Peak contact-metamorphic aureole, Utah, USA. Earth and Planetary Science Letters, 119, 539–559.
Nabelek, P.I., Denison, J.R., and Glascock, M.D. (1990) Behavior of boron during contact metamorphism of calc-silicate rocks at Notch Peak, Utah. American Mineralogist, 75 (7–8), 874–880.
Nabelek, P.I., Labotka, T.C., O'Neil, J.R., and Papike, J.J. (1984) Contrasting fluid/rock interaction between the Notch Peak granitic intrusion and argillites and limestones in western Utah: Evidence from stable isotopes and phase assemblages. Contributions to Mineralogy and Petrology, 86, 25–34.
Pankow, J.F. (1991) Aquatic Chemistry Concepts. Lewis Publishers Inc., Michigan. 673 p.
Pertsev, N.N. (1971) The parageneses of boron in magnesian skarns. Nauka, Moscow (in Russian).
Pichavant, M. and Manning, D.C. (1984) Petrogenesis of tourmaline granites and topaz granites: the contribution of experimental data. Physics of the Earth and Planetary Interiors, 35, 31–50.
Pouchou, J.P. and Pichoir, F. (1987) Basic expression of "PAP" computation for quantitative EPMA. In Eleventh International Congress on X-ray Optics and Microanalysis. University of Western Ontario, London, Ontario, 249–253.
Roedder, E. (Ed.) (1984) Fluid inclusions, 12, 646 p. Reviews in Mineralogy, Mineralogical Society of America, Washington, D.C.
Romer, R.L. and Heinrich, W. (1998) Transport of Pb and Sr in leaky aquifers of the Bufa del Diente metamorphic aureole, north-east Mexico. Contributions to Mineralogy and Petrology, 131, 155–170.
Shabynin, L.I. (1962) Contact metasomatic boron deposits in magnesian skarns. Economic Geology, 57, 1141.
Shaw, D.M., Higgins, M.D., Truscott, M.G., and Middleton, T.A. (1988a) Boron contamination in polished thin sections of meteorites: Implications for other trace element studies by alpha-track image or ion-microprobe. American Mineralogist, 73, 894–900.
Shaw, D.M., Truscott, M.G., Gray, E.A., and Middleton, T.A. (1988b) Boron and Lithium in high-grade rocks and minerals from the Wawa-Kapuskasing region, Ontario. Canadian Journal of Earth Science, 25, 1485–1502.
Skinner, B.J. (1997) Hydrothermal mineral deposits: what we do and don't know. In H.L. Barnes, Ed., Geochemistry of Hydrothermal Ore Deposits, 3rd edition, p. 1–30. Wiley New York.
Smith, R.K. (1972) The mineralogy and petrology of the contact metamorphic aureole around the Alta Stock, (Salt Lake County) Utah. Ph.D. dissertation, University of Iowa, U.S.A.
Sykes, D., Rossman, G.R., Veblen, D.R., and Grew, E.S. (1994) Enhanced H and F incorporation in borian olivine. American Mineralogist, 79, 904–908.
Truscott, M.G. and Shaw, D.M. (1984) Boron in chert and Precambrian siliceous iron formations. Geochimica et Cosmochimica Acta, 48, 2313–2320.
Truscott, M.G., Shaw, D.M., and Cramer, J.J. (1986) Boron abundance and localization in granulites and the lower continental crust. Bulletin of the Geological Society of Finland, 58–1, 169–177.
Watanabe, T. (1967) On kotoite and suanite. In Geology and mineral resources of the Far East, University of Tokyo Press, 1, 236–267.
Watanabe, T., Kato, A., and Katsura, T. (1963) Kotoite, $Mg_3(BO_3)_2$, from the Neichi mine, Iwate prefecture, Japan. Proceedings of the Japanese Academy, 39, 164–169.
Wilson, J.C. (1961) Geology of the Alta Stock, Utah. Ph.D. dissertation, Pasadena, California, California Institute of Technology, 236 p.
Woodford, D.T. (1995) Boron metasomatism in the Alta stock contact aureole, Utah. M.A. Thesis, Houston, Texas, Rice University, 157 p.
Wright, J.E. and Wooden, J.L. (1991) New Sr, Nd and Pb isotopic data from plutons in the northern Great Basin: Implications for the crustal structure and granite petrogenesis in the hinterland of the Sevier thrust belt. Geology, 19, 457–460.
Zhang, Y.G. and Frantz, J.D. (1987) Determination of the homogenization temperatures and densities of supercritical fluids in the system NaCl-KCl-$CaCl_2$-H_2O using synthetic fluid inclusions. Chemical Geology, 64, 335–350.

MANUSCRIPT RECEIVED DECEMBER 2, 1999
MANUSCRIPT ACCEPTED DECEMBER 1, 2000
MANUSCRIPT HANDLED BY PETER I. NABELEK